Natural Resources Canada
Ressources naturelles Canada

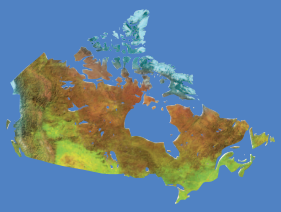

Insights on the geology of the world-class Roberto gold deposit, Éléonore property, James Bay area, Quebec

J.-F. Ravenelle, B. Dubé, M. Malo, V. McNicoll, L. Nadeau, and J. Simoneau

Geological Survey of Canada

Current Research 2010-1

2010

Canada

Geological Survey of Canada
Current Research 2010-1

Insights on the geology of the world-class Roberto gold deposit, Éléonore property, James Bay area, Quebec

J.-F. Ravenelle, B. Dubé, M. Malo, V. McNicoll, L. Nadeau, and J. Simoneau

2010

ISSN 1701-4387
Catalogue No. M44-2010/1E-PDF
ISBN 978-1-100-14588-4
DOI 10.4095/261482

A copy of this publication is also available for reference in depository libraries across Canada through access to the Depository Services Program's Web site at http://dsp-psd.pwgsc.gc.ca

A free digital download of this publication is available from GeoPub: http://geopub.nrcan.gc.ca/index_e.php

Toll-free (Canada and U.S.A.): 1-888-252-4301

Recommended citation

Ravenelle, J.-F., Dubé, B., Malo, M., McNicoll, V., Nadeau, L., and Simoneau, J., 2010. Insights on the geology of the world-class Roberto gold deposit, Éléonore property, James Bay area, Quebec; Geological Survey of Canada, Current Research 2010-1, 26 p.

Critical reviewer
P. Mercier-Langevin

Authors

J.-F. Ravenelle
(jean-francois.ravenelle@ete.inrs.ca)
M. Malo
(michel.malo@ete.inrs.ca)
INRS-ETE
490, rue de la Couronne
Québec, Quebec G1K 9A9

B. Dubé
(bdube@nrcan.gc.ca)
L. Nadeau
(lnadeau@nrcan.gc.ca)
Geological Survey of Canada
490, rue de la Couronne
Québec, Quebec G1K 9A9

V. McNicoll
(vmcnicoll@nrcan.gc.ca)
Geological Survey of Canada
601 Booth Street
Ottawa, Ontario K1A 0E8

J. Simoneau
(jacques.simoneau@goldcorp.com)
Opinaca Mines Ltd./Goldcorp Inc.
853, boul. Rideau
Rouyn-Noranda, Quebec J9X 5B7

Correction date:

Insights on the geology of the world-class Roberto gold deposit, Éléonore property, James Bay area, Quebec

J.-F. Ravenelle, B. Dubé, M. Malo, V. McNicoll, L. Nadeau, and J. Simoneau

Ravenelle, J.-F., Dubé, B., Malo, M., McNicoll, V., Nadeau, L., and Simoneau, J., 2010. Insights on the geology of the world-class Roberto gold deposit, Éléonore property, James Bay area, Quebec; Geological Survey of Canada, Current Research 2010-1, 26 p.

Abstract: The world-class Roberto gold deposit is an atypical gold deposit located in an underexplored part of the Superior Province. The purpose of this paper is to present a preliminary geological description of the deposit and provide insights on geological features that may have played a role in its formation and can be used to help exploration programs. The deposit is located within a kilometre-scale F_2 fold hinge that affects upper-greenschist to amphibolite-facies turbiditic metagreywacke and paragneiss. Gold mineralization is primarily confined to a series of subparallel decametre-scale-wide mineralized zones and is associated with a hydrothermal system characterized by calc-silicate-bearing veins and metasomatic replacement zones, potassic alteration, and tourmaline. The principal mineralized zone (Roberto) consists of a stockwork of quartz±actinolite±diopside±biotite-arsenopyrite-pyrrhotite veins and quartz-dravite-arsenopyrite veinlets, contained within quartz-microcline (potassic alteration)-phlogopite-biotite and dravite replacement zones. While most of the alteration and mineralized zones are deformed by structures attributed to D_2, some occurrences appear to be controlled by D_2 structures; gold mineralization is thus interpreted as being pre- or early-D_2. Although geochronological data permit to refute the hypothesis that the Roberto deposit (<2675 ± 6 Ma) is associated with the nearby Ell Lake diorite (2705 ± 1.9 Ma), the potential input from magmatic fluids should not be blindly discarded, as indicated by the presence of potentially younger porphyritic intrusions and multiple generations of pegmatite bodies, some of which being potentially contemporaneous with a part of the mineralization or its remobilization.

Résumé : Le gisement aurifère de classe mondiale Roberto est un gisement d'or atypique situé dans une région sous-explorée de la Province du lac Supérieur. Le but de cet article est d'offrir une description géologique préliminaire du gisement et de fournir une vue des caractéristiques géologiques qui ont pu jouer un rôle dans la formation du gisement et dont la connaissance pourrait être utile à la conduite des programmes d'exploration. Le gisement est situé dans la charnière d'un pli P_2 d'échelle kilométrique qui affecte des métagrauwackes turbiditiques et des paragneiss métamorphisés dans des conditions du faciès des schistes verts supérieur au faciès des amphibolites. La minéralisation aurifère est principalement contenue dans une série de zones décamétriques subparallèles et est associée à un système hydrothermal caractérisé par des veines et des zones de remplacement riches en calcium, de l'altération potassique et de la tourmaline. La zone minéralisée principale (Roberto) est composée d'un stockwerk de veines de quartz±actinote±diopside±biotite-arsénopyrite-pyrrhotite et de veinules de quartz-dravite-arsénopyrite contenues dans des zones de remplacement riches en quartz-microcline (altération potassique)-phlogopite-biotite et en dravite. Alors que la majeure partie de l'altération et des zones minéralisées est déformée par la déformation D_2, certaines zones semblent contrôlées par D_2. La minéralisation aurifère est donc interprétée comme s'étant mise en place avant ou tôt dans D_2. Bien que les travaux de géochronologie démontrent que l'intrusion dioritique du lac Ell (2705 ± 1,9 Ma), située à proximité du gisement Roberto, est trop ancienne pour avoir contribué à la formation du gisement (<2675 ± 6 Ma), le rôle possible de fluides magmatiques ne peut être éliminé, notamment en raison de la présence d'autres intrusions porphyriques potentiellement plus jeunes et de plusieurs générations de pegmatites dont certaines pourraient être contemporaines d'une partie de la minéralisation ou de sa remobilisation.

INTRODUCTION

The Roberto gold deposit represents one of the most significant discoveries of the past 10 years in Canada. This multimillion ounce gold deposit was discovered by Virginia Gold Mines Inc. (now Virginia Mines Inc.) in 2003 on their Éléonore property located in the James Bay region of northwestern Quebec (Fig. 1). The James Bay area then rapidly became a key target for gold exploration because of its potential to host a new gold district. In May 2006, Goldcorp Inc. acquired 100% of the property with the intention of putting the deposit into production through their Opinaca Mines Ltd. wholly owned subsidiary. Since then, Opinaca Mines Ltd. ran an intensive drilling program in order to better define the extent of mineralized zones. The latest resource estimation (publicly released in February 2010) indicated a total of more than 9 million ounces (280 t) of inferred (6.25 Moz, 194 t) and indicated (3.15 Moz, 98 t) resources (Goldcorp Inc., 2010).

The geology of the Roberto deposit differs from most Canadian Archean gold deposits of the southern Superior Province in that it is characterized by stockwork- and

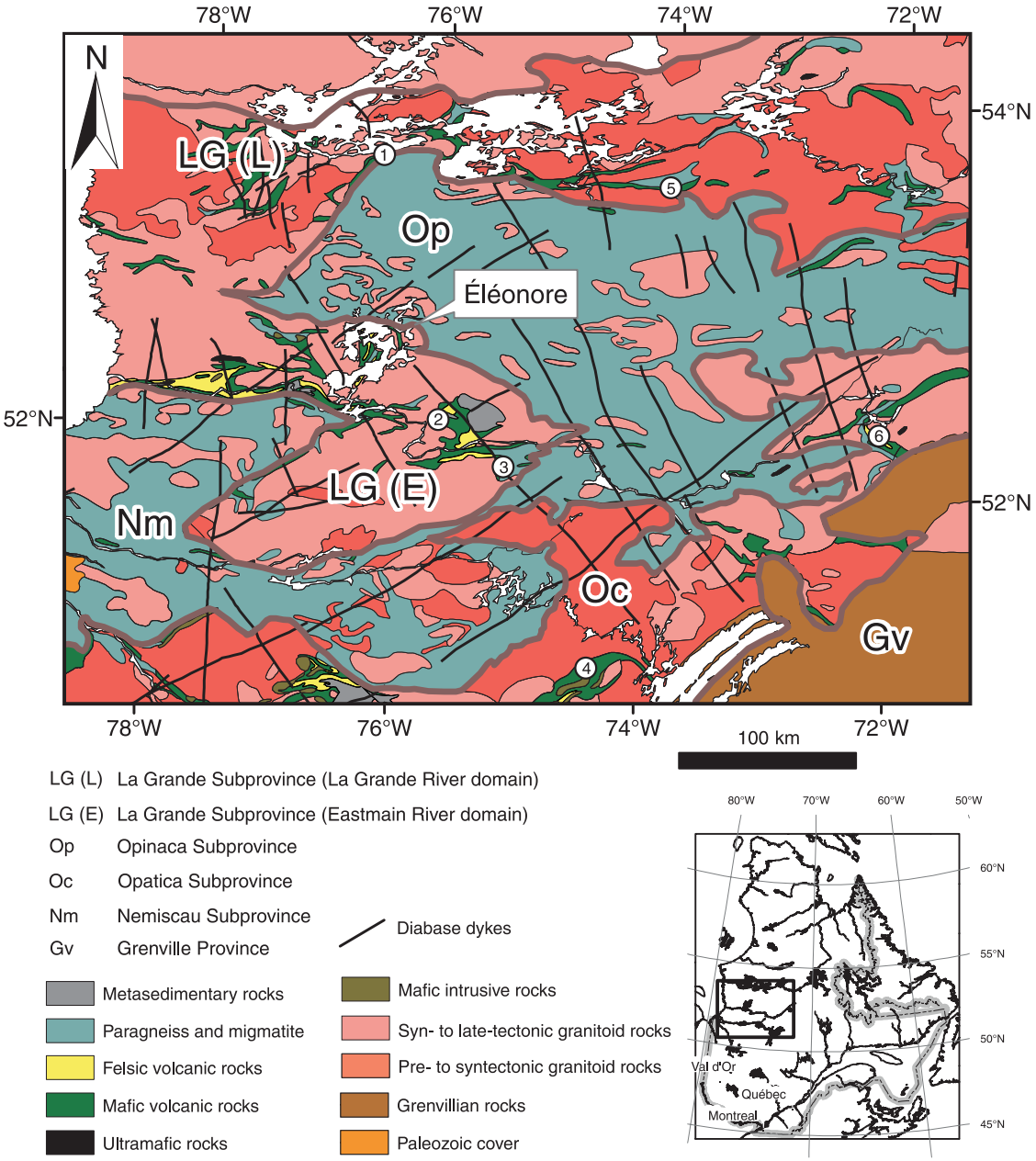

Figure 1. Subprovince-scale geological map showing the location of the Éléonore property. Circled numbers indicate location of significant gold prospects and deposits in the region: 1 = La Grande Sud, 2 = Clearwater, 3 = Auclair, 4 = Troilus mine, 5 = Corvet Est, 6 = Eastmain mine (modified from Thériault and Bilodeau, 2001).

replacement-style mineralization hosted within amphibolite-facies turbiditic metagreywacke and paragneiss. Contrary to the well studied and well explored Abitibi greenstone belt of the Superior Province, gold exploration in the James Bay area is more recent and the level of geological information more limited. Hence, the Roberto deposit represents a milestone for future gold exploration within the northern part of the Superior Province. Being an atypical gold deposit located in a relatively underexplored territory, however, the key geological parameters involved in its genesis need to be identified in order to understand its formation, location, and geometry, and to define exploration criteria that will help discover other mineralized zones on the property and/or potentially similar gold deposits in the James Bay area and elsewhere in amphibolite-grade terranes of the Superior Province.

The study of gold deposits in polydeformed terranes is generally complex due to the common protracted deformational, metamorphic, and magmatic history of the geological setting and the difficulty to determine the timing of gold deposition. Accordingly, the purpose of this report is to present a preliminary geological description of the Roberto gold deposit and provide insights on geological features that may have played a role in its formation and can be used to help exploration programs. Using regional and local geological mapping, structural analysis, core logging, 3-D Gocad reconstructions, petrography, and geochronology, efforts are focused on acquiring an understanding of the geology, the relative ages of the main lithological units, and the mineralogical and geochemical characteristics of the deposit. An emphasis is also put on determining the relative chronology between gold mineralization, tectono-metamorphic events, and magmatic phases.

REGIONAL AND LOCAL GEOLOGICAL SETTING

The Éléonore property straddles the contact between the amphibolite- to granulite-facies metasedimentary Opinaca Subprovince and the Eastmain River domain of the greenschist- to amphibolite-facies volcano-plutonic La Grande Subprovince (Fig. 1). The La Grande Subprovince is crescent shaped and surrounds the south, west, and north borders of the Opinaca Subprovince (Fig. 1). The northern and southern parts of the La Grande Subprovince are referred to as the La Grande River and Eastmain River domains, respectively (Gauthier and Larocque, 1998) (Fig. 1). The two subprovinces have distinct metamorphic grades and therefore most probably have different rheological behaviour, which potentially explains the more ductile deformational style of the Opinaca Subprovince. Although the contact between the La Grande River domain of the La Grande and the Opinaca subprovinces is interpreted to correspond to a tectonic contact where La Grande Subprovince volcanic rocks were thrust onto younger Opinaca Subprovince paragneiss (Goutier et al., 1996; Paquette and Gauthier, 1997; Gauthier et al., 1997), no tectonic structure juxtaposing rocks of different metamorphic grades has been clearly documented at the contact between the Eastmain River domain of the La Grande and the Opinaca subprovinces. Gauthier and Larocque (1998) therefore assigned the Eastmain River domain–Opinaca Subprovince contact to the metamorphic isograd that separates the paragneiss units from the underlying greywacke sequences. As proposed by Franconi (1978), it is hence interpreted that sedimentary rocks located at the top of the La Grande Subprovince stratigraphy and higher grade sedimentary rocks of the Opinaca Subprovince are part of a continuous conformable sequence. On the other hand, it was recently proposed that a break observed in the magnetic grain of a recent regional-scale airborne magnetic survey could represent a tectonic boundary separating the two subprovinces (D. Bandyayera, C. Maurice, P. Rhéaume, and P. Keating, work presented at Quebec Exploration Conference, Québec, Quebec, November 25, 2008). Even though more work is required to define the nature of the inferred break and determine if it has any tectonic significance, this scenario offers an alternate explanation for the juxtaposition of two terranes with different deformational and metamorphic attributes. The Roberto deposit is hosted in La Grande Subprovince metasedimentary rocks, a few kilometres south of the boundary between the two subprovinces (Fig. 2), and is hence located relatively close to the tectonic boundary inferred by D. Bandyayera and others (D. Bandyayera, C. Maurice, P. Rhéaume, and P. Keating, work presented at Quebec Exploration Conference, Québec, Quebec, November 25, 2008).

Opinaca Subprovince

The Opinaca Subprovince is mainly composed of migmatized metasedimentary rocks intruded by syn- to post-tectonic granodiorite and granitic pegmatite intrusions (Fig. 2) that have a peraluminous signature indicative of S-type granitoid rocks derived from partial melting of sedimentary rocks (Moukhsil et al., 2003). The youngest ages for such intrusions are 2618 +18/-13 Ma obtained for the Du Vieux Comptoir granite, located about 85 km west of the Roberto deposit, and 2618 ± 2 Ma for a pegmatitic tonalite in the Lac Sakami region, located about 75 km northwest of the Roberto deposit (David and Parent, 1997). Local ultramafic intrusions have recently been documented (Bandyayera and Fliszár, 2007), and thin volcanic units were locally mapped (Franconi, 1983; Simard and Gosselin, 1999). Metamorphic grade systematically increases from amphibolite facies near the margins to granulite facies in the centre of the Opinaca basin (Moukhsil et al., 2003).

La Grande Subprovince

The Eastmain River domain of the La Grande Subprovince consists of greenschist- to amphibolite-facies volcanic and metasedimentary rocks intruded by synvolcanic

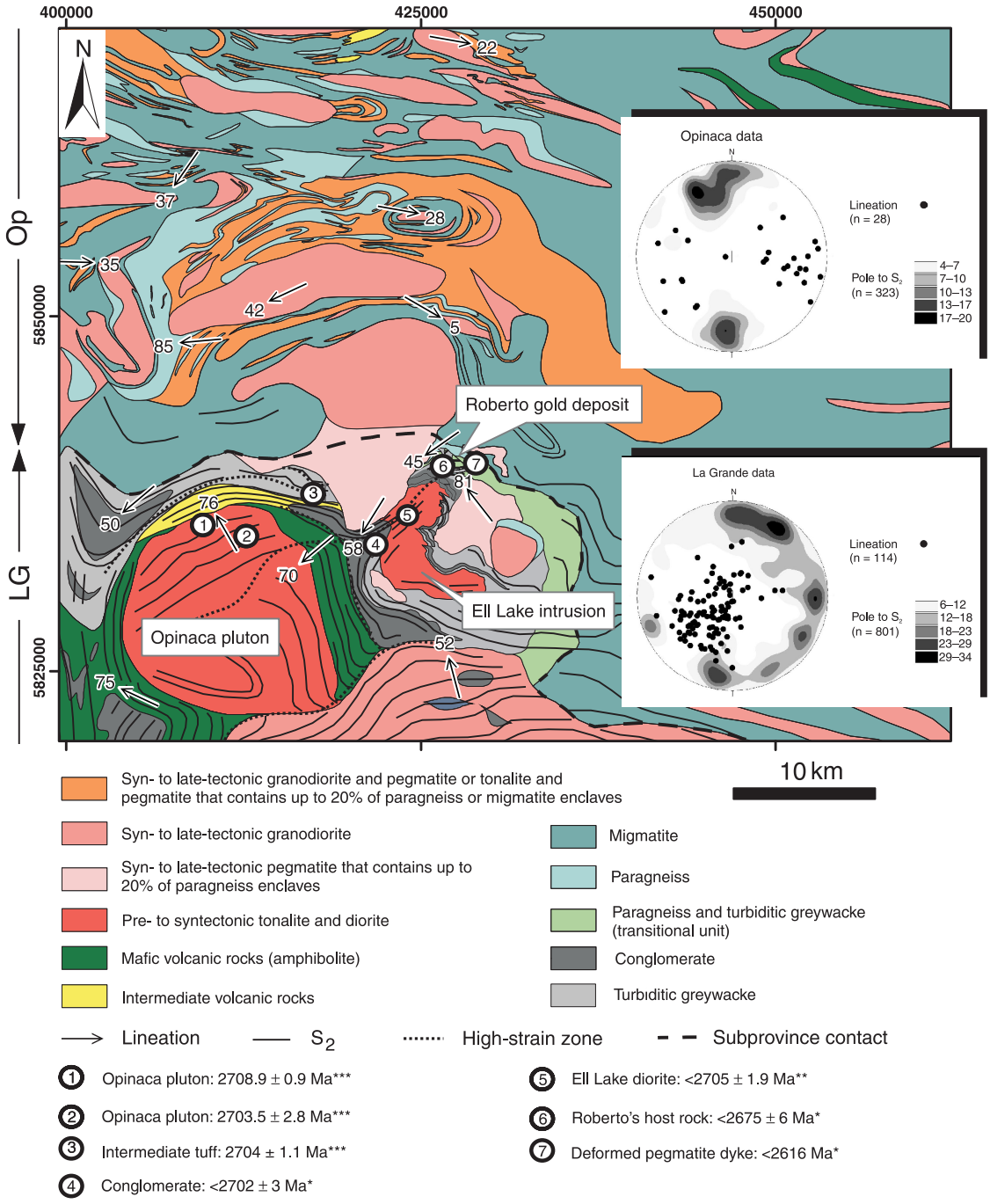

Figure 2. Regional geological setting of the Roberto gold deposit (*modified from* maps RP 2007-05-C001 and RP 2007-05-C002 of Bandyayera and Fliszár (2007). Equal area nets (lower hemisphere) show the distribution of lineation and S_2 foliation measurements for the La Grande (LG) and Opinaca (Op) subprovinces. Selected lineation measurements are represented on the map. Note the shallower plunges of lineations within the Opinaca Subprovince. Structural data selected from Bandyayera and Fliszár (2007) and this study. Circled numbers show location of geochronological samples (*this study, ** J. David (unpub report for Virginia Mines Inc., 2005), *** Bandyayera and Fliszár (2007)). Co-ordinates are in UTM NAD 83.

and syntectonic tonalite, granodiorite, and diorite intrusions dated between 2747 Ma and 2710 Ma (Moukhsil et al., 2003). The volcanic sequence is composed of four cycles of tholeiitic volcanism dated between 2752 Ma and 2703 Ma that generated komatiitic to rhyolitic lavas and tuffs with local calc-alkaline affinities (Kauputauch, Natel, Anatacau-Pivert, and Komo-Kasak formations) (Moukhsil et al., 2003). Older komatiite units, related sills (2.82 Ga), and Mesoarchean basement (3.33–2.79 Ga) are present in the western part of the La Grande Subprovince (Percival, 2007). The volcanic sequence is overlain by conglomerate and turbiditic greywacke units locally containing volcaniclastic and tuffaceous sequences and minor iron-formation units (Clarkie and Anaconda formations) (Moukhsil et al., 2003). Franconi (1978) suggested that the conglomerate sequences were unconformably deposited on top of the volcanic pile and represent the base of the sedimentary sequence. Felsic volcanic and volcaniclastic rocks associated with quartz-feldspar porphyry bodies (Wabamisk Formation) dated at 2703 ± 8 Ma and 2705 ± 3 Ma (Gauthier and Larocque, 1998) are locally present between the mafic volcanic rocks and the sedimentary sequence (Franconi, 1978; Gauthier and Larocque, 1998). Metamorphic grade increases upstratigraphy (Gauthier and Larocque, 1998) as illustrated by greywacke units that gradually develop paragneissic fabrics toward the contact with the Opinaca Subprovince.

In the vicinity of the Éléonore property, La Grande supracrustal rocks consist of locally pillowed basalt units and minor intermediate to felsic lapilli tuff units of the Kasak Formation, which are overlain by conglomerate units dominated by rounded centimetre- to decimetre-scale diorite blocks (Fig. 2). The map pattern and the presence of basaltic and tuffaceous blocks observed within conglomerate units strongly suggests that the conglomerate units were unconformably deposited on top of the volcanic rocks, as proposed by previous workers elsewhere in the subprovince (e.g. Franconi, 1978; Labbé and Grant, 1998). This clastic sequence comprising conglomerate and turbiditic greywacke units is referred to as the Low Formation, and could correspond to Labbé and Grant's (1998) Clarkie Formation (Bandyayera and Fliszár, 2007). The local presence of andalusite-cordierite-garnet assemblages within the Low Formation (Bandyayera and Fliszár, 2007) potentially reflects the local pelitic character of this formation. The supracrustal sequence is cut by the large synvolcanic tonalitic to dioritic Kasipasikatch intrusion (renamed Opinaca pluton by Bandyayera and Fliszár (2007)) and the tonalitic to dioritic Ell Lake intrusion (Fig. 2). The Ell Lake intrusion is of particular importance, since it contains Cu-Ag-Au-Mo mineralization, and its northern boundary is located only 3 km southwest of the Roberto deposit. Later syn- to post-tectonic granodiorite and pegmatite intrusions most probably associated with migmatization of the Opinaca basin also intrude La Grande Subprovince rocks and locally form kilometre-scale intrusions (Fig. 2).

Structural geology

Evidence for three generations of structures (D_1 to D_3) is found in the Eastmain domain of the La Grande Subprovince (Moukhsil et al., 2003; Bandyayera and Fliszár, 2007), but only two are found in the Opinaca Subprovince (D_2 and D_3). The first deformational event (D_1) was documented in the Secteur Village (NTS 33 B/3) and Lac Duxbury (NTS 33 C/5) areas (Moukhsil et al., 2003). In the present study area, structures attributed to D_1 are cryptic, and reside in the presence of local intrafolial folds (Bandyayera and Fliszár, 2007) or minor F_1 folds refolded by F_2 folds. Previous studies labelled the main deformational event as D_1 instead of D_2 (e.g. Franconi, 1978; Moukhsil, 2000). It should be noted that evidence of D_1 was not found in the turbiditic sequence that hosts the Roberto deposit. This section describes the principal characteristics of D_2 and D_3 structures in both the La Grande and Opinaca subprovinces as established from collaborative work with Bandyayera and Fliszár (2007).

La Grande Subprovince

The main regional deformation responsible for the predominant approximately east-west structural fabric that affects prograde metamorphic minerals is attributed to D_2 (Bandyayera and Fliszár, 2007). The S_2 fabric is penetrative and is generally oriented subparallel to primary layering of volcanic and sedimentary sequences. In the study area, the attitude of S_2 is greatly influenced by competent intrusive bodies, as can be seen around the Opinaca pluton, where the fabric both affects the intrusion and moulds the outline of the intrusion (Fig. 2). F_2 folds are moderately to steeply plunging, tight to isoclinal folds and are commonly associated with well developed stretching and mineral lineation oriented subparallel to their fold axis. Areas of intense stretching represented by the presence of L-tectonite structures are common and indicate that D_2 locally caused significant constrictional strain. Several kilometre-scale northeast- and northwest-striking high-strain zones are present and locally show intense flattening strain generally associated with a well developed downdip lineation. Lineations associated with the high-strain zones are oriented subparallel to the L_2 regional lineation, which indicates that the high-strain zones are in part compatible with D_2. Dragging of S_2 along the high-strain zones suggests that the zones were still active during the latest stages of D_2. The third deformational event (D_3) generated a conjugate set of folds associated with east-northeast- and west-northwest-striking axial planes that are steeply plunging and near coaxial with F_2 folds. S_3 is generally penetrative and locally realigned metamorphic minerals initially affected by S_2.

Opinaca Subprovince

The S_2 fabric can be traced across the metamorphic isograd that separates the La Grande and the Opinaca subprovinces, where it gradually develops into a paragneissic fabric and/or migmatitic layering. As mentioned by Simard and Gosselin (1999), this suggests that high-grade metamorphism associated with migmatization of Opinaca Subprovince sedimentary rocks was synchronous with D_2. The presence of late anatexic injections locally discordant to the main fabric suggests that migmatization was ongoing throughout D_2 and perhaps outlasted D_2 (Simard and Gosselin, 1999). The primary layering and the S_2 fabric are locally refolded by tight, doubly plunging folds which reorient L_2 lineations to shallower plunges and result in the formation of dome-and-basin structures (Fig. 2). These later folds are primarily interpreted to result from D_3, although local doming associated with diapiric emplacement of syn- to late-tectonic intrusions might also be responsible for the finite geometry of the Opinaca Subprovince (Bandyayera and Fliszár, 2007). Such F_3 folds are generally not associated with an axial-planar fabric, although axial-planar crenulation cleavages have locally been documented.

Ell Lake diorite Cu-Au-Ag mineralization

The Ell Lake intrusion (2705 ± 1.9 Ma; J. David (unpub. report for Virginia Mines Inc., 2005)) is host of several Cu-Au-Ag showings that are located 7 km southwest of the Roberto deposit (Fig. 2). The characteristics and the relative timing of these intrusion-hosted mineralizations are currently under study (Bécu et al., 2007). The intrusion consists of dioritic and tonalitic phases locally cut by feldspar-porphyry dykes. The mineralized zones are generally associated with semimassive to massive chalcopyrite±pyrrhotite impregnations, disseminations, and replacement with rare traces of molybdenite. Prominent tourmaline alteration zones that resemble Roberto's tourmaline-rich stockwork (*see* below) are present in the vicinity of the mineralized zones, which may suggest that mineralization at Roberto and at the Ell Lake diorite share some common attributes and could be related. Several submetric high-strain zones and well developed downdip lineation (L_2) on foliation planes have been mapped in the area. During the course of this study, the potential genetic relationship between the Ell Lake diorite and the Roberto deposit was investigated through geochronology.

GEOLOGY OF THE ROBERTO DEPOSIT

This section presents a preliminary description of the main lithological, structural, alteration, and mineralization characteristics of the Roberto deposit based on data from hundreds of drill holes, local stripped outcrops, and a very large stripped outcrop (100 m x 400 m) excavated by Opinaca Mines Ltd. in the core of the deposit (Fig. 3, 4a).

Lithology

The Roberto deposit is hosted by upper-greenschist to lower-amphibolite facies sequences of the Low Formation, which includes turbiditic greywacke, conglomerate units locally interbedded with arenite, aluminosilicate-porphyroblast-bearing units, biotite schist units (locally auriferous) (Fig. 3), minor banded cherty iron-formation units, and paragneiss. Since the bulk of the deposit is submerged under water, the distribution of lithological units presented on Figure 3 is primarily based on drill-core data. The lithologies are cut by a swarm of pegmatite dykes which are on average less than 1 m wide and up to hundreds of metres in length. Spatial relationships between pegmatite dykes and paragneiss units are locally observed, especially on drill sections. These spatial relationships suggest that some of the paragneiss units were generated in association with pegmatite dyke emplacement. A small feldspar porphyry intrusion is located in the northern part of the deposit (Fig. 3), and minor feldspar porphyry dykes are locally documented. Proximal to the migmatized Opinaca Subprovince to the east, paragneiss units become more abundant, as regional metamorphic grade gradually increases. These paragneiss units are biotite-rich and locally contain aluminosilicate porphyroblasts.

Structural geology

The Roberto deposit occurs within a kilometre-scale, subvertically plunging F_2 synformal anticline (Fig. 5). The vertical extent of the folded geometry and mineralized system has been traced to 1500 m below surface. The detailed geometry of the kilometre-scale fold and the distribution of lithological units, alteration assemblages, and mineralized zones are complex (Fig. 3). This is especially the case for the aluminosilicate-porphyroblast-bearing sequences, the thickness of which varies significantly within the fold hinge (Fig. 3, 5), and for conglomerate and arenitic units, which are discontinuous (Fig. 3).

The overall style of the kilometre-scale fold is similar to decametre- to metre-scale, tight to isoclinal parasitic F_2 folds commonly documented on outcrops (Fig. 6a). F_2 folds are not always associated with an axial-planar fabric, as minerals affected by S_2 are commonly recrystallized and/or reoriented parallel to the flattening plane associated with D_3. As a result, it is common to observe a penetrative S_3 fabric that transects the limbs of a given F_2 fold, without seeing evidence of an axial-planar S_2 fabric (Fig. 6b). Nonetheless, crenulation of S_2 by S_3 is locally documented, specifically in paragneiss units where S_2 is strongly developed. Overprinting relationships between S_2 and S_3 are well illustrated within aluminosilicate-bearing rocks, where on a given outcrop aluminosilicate porphyroblasts affected by S_2 are crenulated by S_3 in one location, but are reoriented parallel to the axial plane of F_3 folds in another location. Such F_3 folds are distinguished from F_2 folds by their more open style of folding (Fig. 6c). Since S_2 and S_3 are defined by the same metamorphic minerals (mainly biotite and aluminosilicate

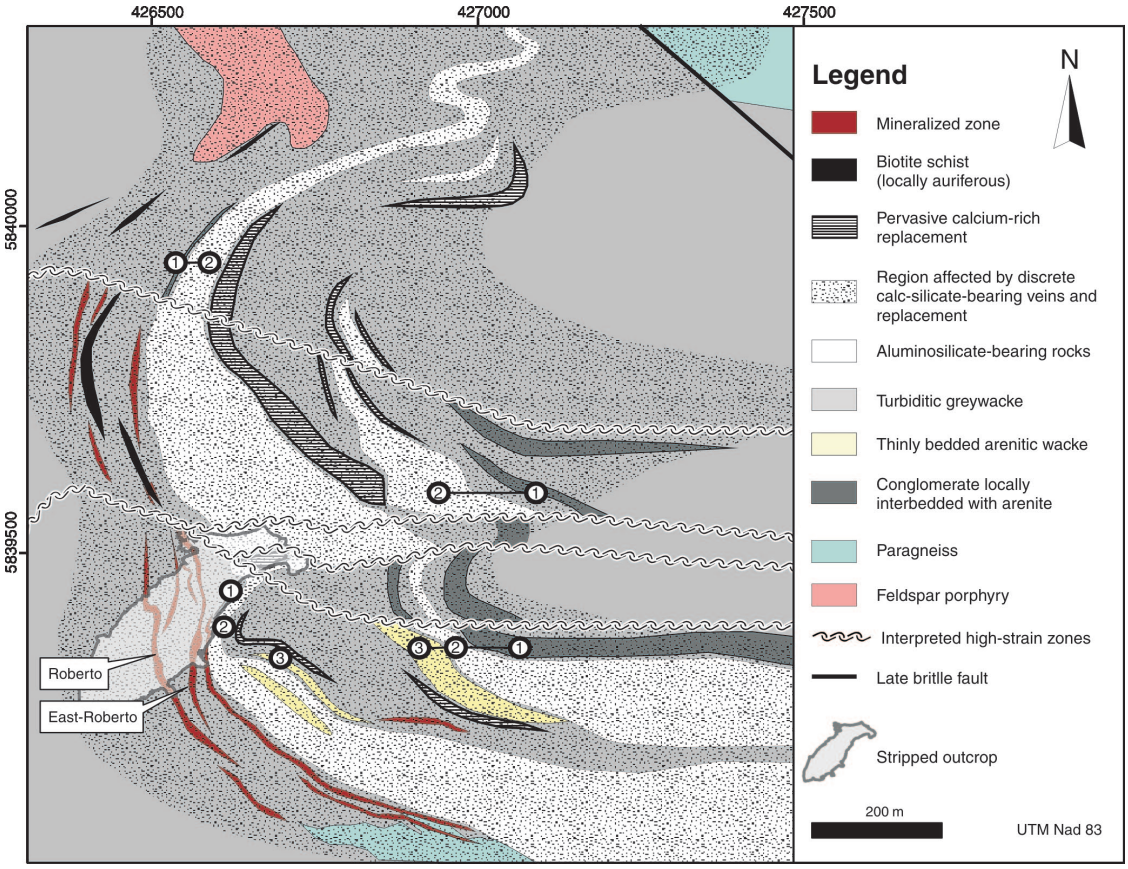

Figure 3. Geological map of the Roberto gold deposit. Note the repetition of lithological units (conglomerate–aluminous rocks–arenitic wacke) identified by the circled numbers (1-2-3, respectively).

porphyroblasts), distinction between the two fabrics in the absence of folds can only be interpeted based on orientation. A 15 m wide D_2 high-strain zone occurs about 1 km to the southwest of the deposit and affects metasomatized conglomerate units (Fig. 2). The linear extrapolation of this high-strain zone bounds the southern limb of the deposit-scale fold.

Stripped outcrop

The very large stripped outcrop enabled the authors to study the distribution of tectonic fabrics and their relationships with the kilometre-scale folded geometry. The distribution of the S_2 fabric on the stripped outcrop is illustrated in Figure 4a. In areas where S_3 overprinted S_2, the attitude of S_2 was deduced from the attitude of F_2 axial planes. The map shows that the trace of S_2 is complex. Field documentation indicates that it is affected by significant slip along fault and/or bedding surfaces, one of which bounds the East-Roberto zone (Fig. 4a). In the northeastern portion of the stripped outcrop (Fig. 4a, circled number 3), the attitude of bedding is east-west and is oriented parallel to S_2 (Fig. 6d), which is not consistent with cleavage-bedding relationships typically observed in fold hinges; however, the presence of preserved F_2 fold hinges with strongly transposed limbs in that region (Fig. 6e) indicates that the sequence has been affected by significant transposition. The 'true' attitude of bedding is alternatively interpreted to correspond to the contact between the massive greywacke and the aluminosilicate-porphyroblast-bearing rocks (Fig. 4a, circled number 4), which is oriented at a high angle to S_2. Note that the attitude of S_3 is more constant, varying from east-northeast to northeast (Fig. 4a).

The attitude of the F_2 fold that affects the global distribution of bedding attitudes on the stripped outcrop was calculated from the distribution of pole to bedding data collected on the outcrop (Fig. 4b). Local estimates of F_2 and F_3 fold axes orientations were calculated from bedding-S_2 and bedding-S_3 intersections, respectively. The distribution of calculated F_2 and F_3 fold axes indicates that F_2 and F_3 folds are coaxial (Fig. 4c). When compared to F_2 and F_3 fold axes, the attitude of lineation measurements collected on S_2 planes (Fig. 4d) are subparallel (Fig. 4e). These lineations represent direct measurements of either the intense stretching associated with D_2 or the trace of S_3 on S_2 planes.

On the northeastern side of the large stripped outcrop, several centimetre- to metre-scale high-strain zones are present and mark the boundary between different lithological units and/or alteration assemblages (Fig. 4a). The

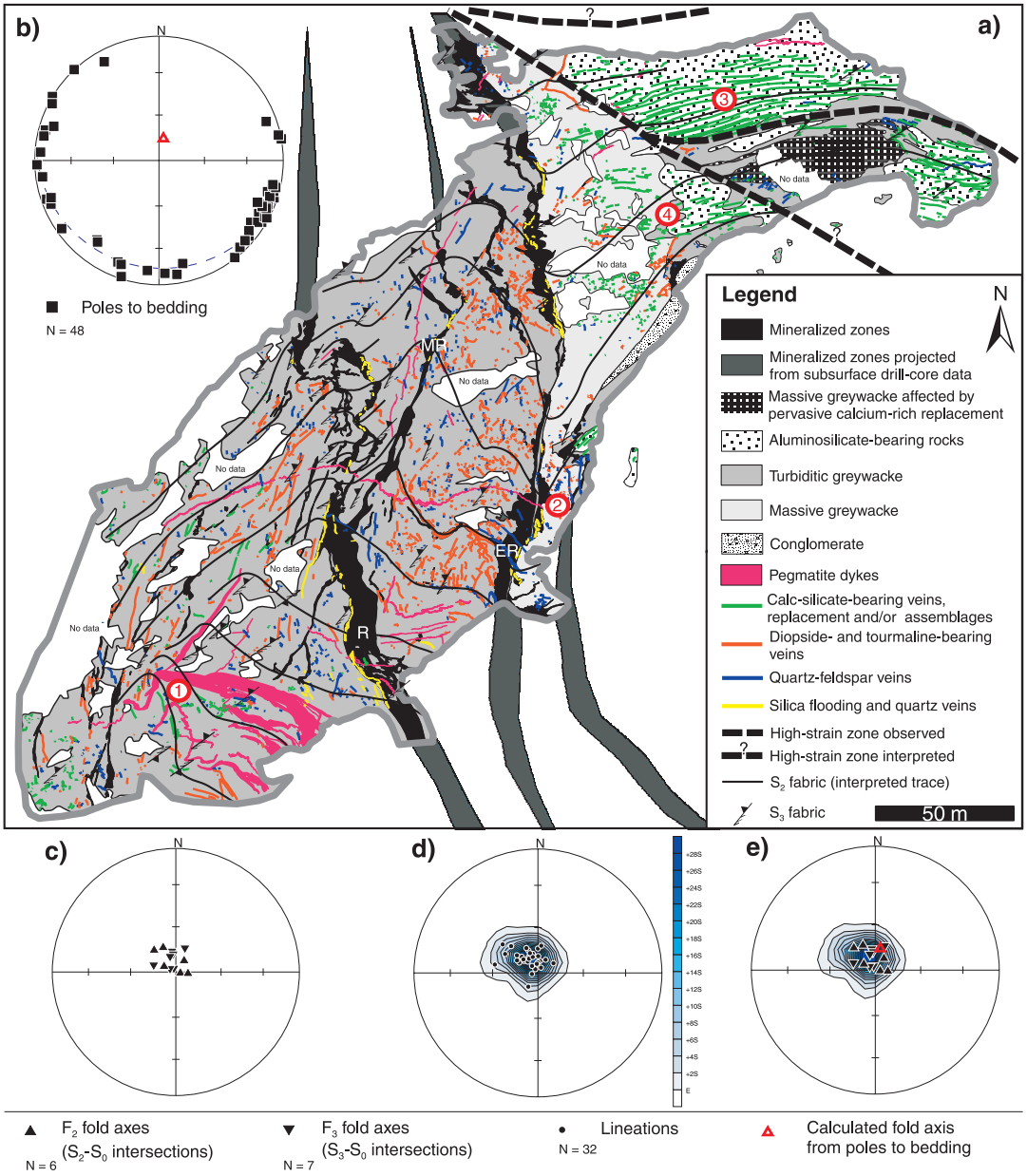

Figure 4. a) Simplified geological map of the very large stripped outcrop exposing the core of the Roberto deposit. Circled numbers: 1 = location of pegmatite dykes folded by F_2 folds, 2 = location of pegmatite dyke that crosscuts slip plane affecting East-Roberto, 3 = location where S_0 is oriented east-west, 4 = contact between massive greywacke and aluminosilicate-bearing rocks (*see* text for details); R = Roberto, MR = Mid-Roberto, ER = East-Roberto. **b), c), d), e)** Equal area nets (lower hemisphere) showing the distribution of structural measurements collected on the outcrop. **b)** Distribution of poles to bedding. The first Eigen vector calculated from the distribution gives an approximation of the fold axis in the folded strata (011°/75°). **c)** Distribution of F_2 fold axes (calculated S_0-S_2 intersections) and F_3 fold axes (calculated S_0-S_3 intersections). **d)** Contoured distribution of lineation. **e)** Synoptic net showing the relative attitudes of the fold axis calculated in Figure 4b, F_2-F_3 fold axes displayed on Figure 4c, and contoured lineations displayed on Figure 4d.

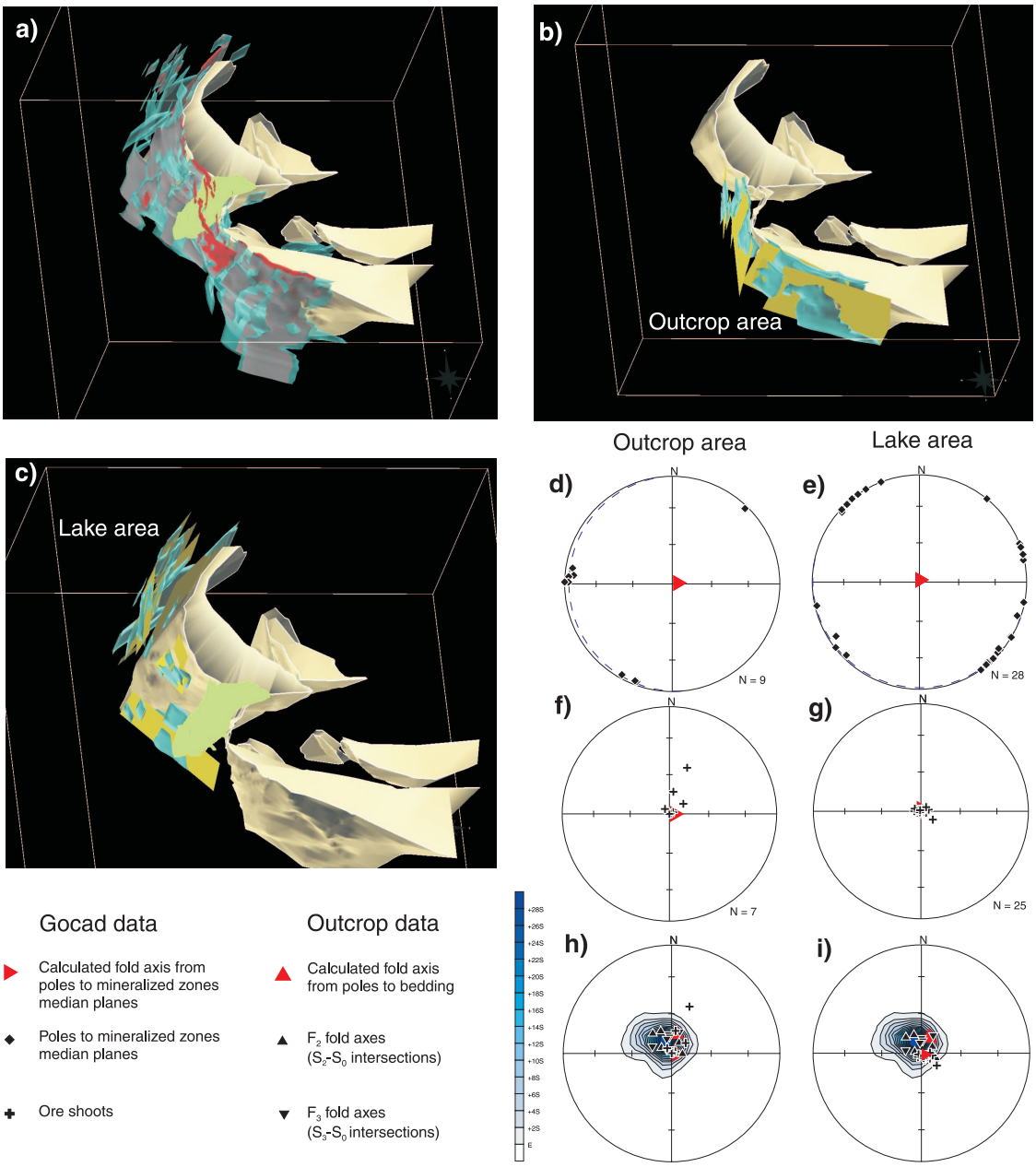

Figure 5. a), **b)**, **c)** 3-D Gocad reconstructions for the first 400 m of the Roberto deposit showing the distribution of mineralized zones (transparent blue), high-grade mineralized zones (red), and aluminosilicate-bearing rocks (pale yellow). Median planes passing through mineralized zones (yellow) and coloured outline of the stripped outcrop (green) are also represented. **a)** General view. **b)** Distribution of selected mineralized zones and associated median planes used to calculate a fold axis for the 'outcrop area'. **c)** Distribution of selected mineralized zones and associated median planes used to calculate a fold axis for the 'lake area'. **d)** to **i)** Equal area nets (lower hemisphere) showing the distribution of structural measurements extracted from Gocad and/or structural measurements collected on the stripped outcrop. **d)**, **e)** Distribution of poles to mineralized zones median planes and calculated fold axis for the 'lake area' (017°/88°) and 'outcrop area' (091°/85°), respectively. **f)**, **g)** Distribution of ore shoot attitudes extracted from Gocad for the 'lake area' and 'outcrop area', respectively. Fold axes calculated in Figures 5d and 5e are also represented for comparison. **h)**, **i)** Synoptic nets showing geometrical relationships between ore shoots, fold axes in mineralized zones calculated from Gocad, fold axis in bedding calculated from outcrop data, and linear measurements (F_2-F_3 fold axes, lineations (coloured contours)) collected on the stripped outcrop.

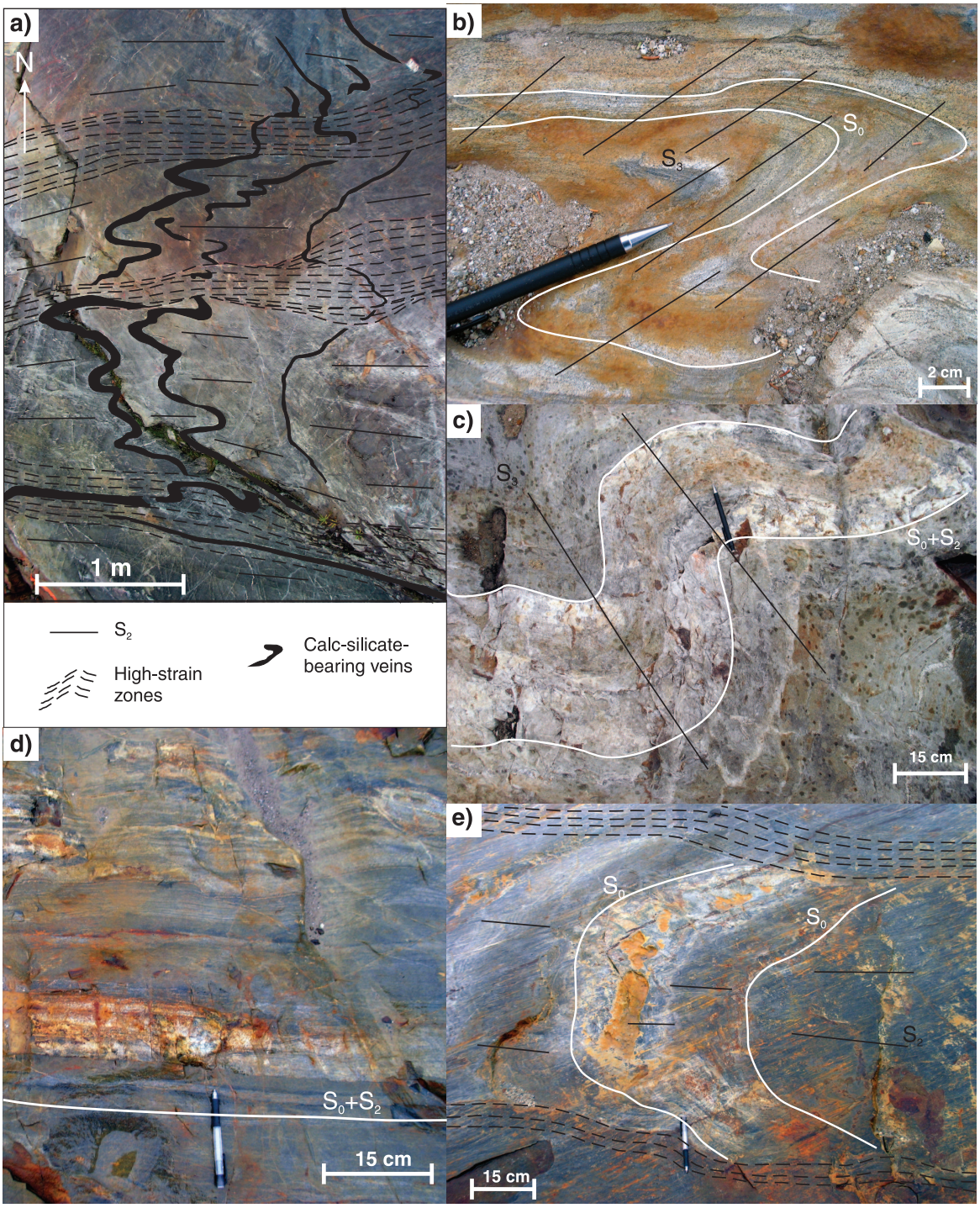

Figure 6. **a)** Interpreted drawing of a photograph of a metre-scale F_2 fold deforming calc-silicate-bearing veins. The style of the fold and the presence of high-strain zones axial planar to the fold resemble the overall style of the kilometre-scale fold that affects the Roberto deposit. The figure represents a mirror image of the original photograph. **b)** Geometrical relationship between an F_2 fold and the only penetrative fabric observed near the fold. The penetrative fabric is interpreted to represent S_3 since it cuts across both limbs of the fold. 2010-013. **c**) F_3 fold in S_0-S_2. Note the more open style of the F_3 fold compared with the F_2 fold portrayed on Figure 6b. 2010-023. **d)** Bedding and bedding-parallel calc-silicate-bearing replacement transposed parallel to S_2. 2010-002. **e)** Preserved F_2 fold hinge in S_0 bounded by centimetre-scale high-strain zones. 2010-001. All photographs by J.-F. Ravenelle.

finite stretching and transport direction on these high-strain zones is interpreted to be subvertical from the attitudes of sheath folds occurring in such high-strain zones (e.g. Fig. 7). Dragging along the high-strain zones might have contributed to the transposition and reorientation of bedding in the north-eastern portion of the stripped outcrop as described above.

Subsurface geometry and ore shoots

The Gocad software was used to represent the 3-D distribution of mineralized zones and aluminosilicate-bearing rocks (Fig. 5a), and perform a structural analysis of the subsurface (Fig. 5). Only the first 400 m were here considered for the structural analysis, as drill-core data are scarce in the deeper level of the deposit. The 3-D representation of Figure 5a shows the presence of two structural domains delimited by the high-strain zones documented on the eastern side of the stripped outcrop. It should be noted that these high-strain zones are not easily recognizable in drill core, and that their deposit-scale 3-D geometry is based on apparent discontinuities in the distribution of lithological units, alteration facies, and mineralized zones. Two domains referred to as 'outcrop area' and 'lake area' are treated separately in the structural analysis of the subsurface.

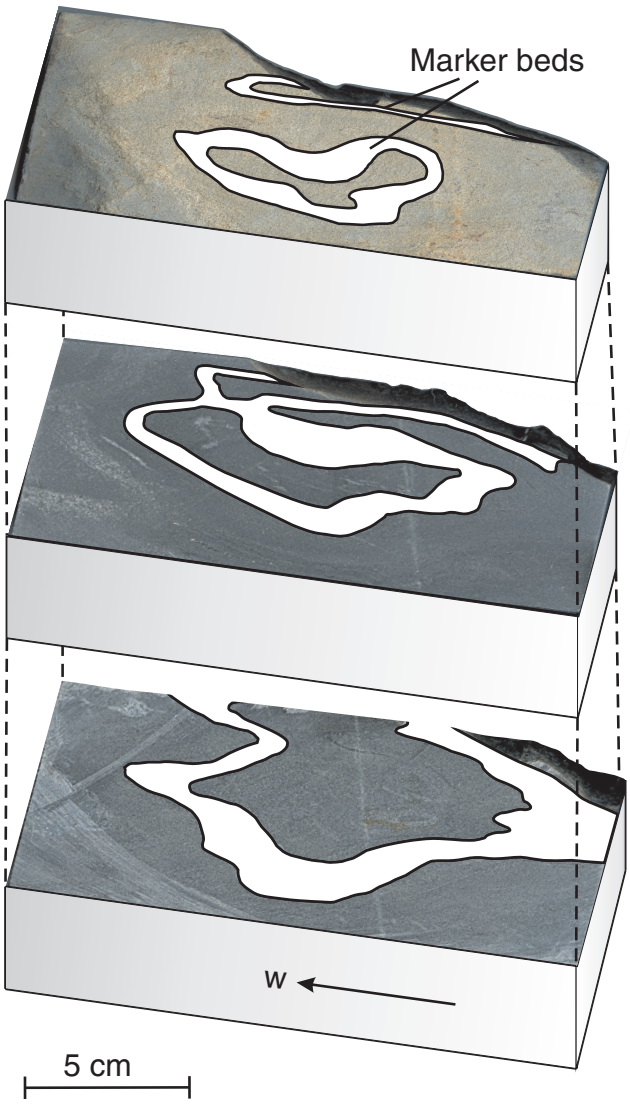

Figure 7. Geometry of sheath folds interpreted from photographs of slices through a hand sample located in a high-strain zone of the large stripped outcrop. The cone axis of the sheath folds is subvertical.

Within mineralized zones, Opinaca Mines Ltd. were able to model the 3-D distribution of high-grade ore shoots, which generally have a much larger vertical than horizontal extension (Fig. 5a). The fact that the ore shoots are commonly vertically elongated suggests that their attitude is structurally controlled. In order to test the hypothesis that the attitude of ore shoots is controlled by the fold axis of the deposit-scale fold, fold axes controlling the global geometry of mineralized zones in the 'outcrop area' and 'lake area', were calculated (Fig. 5d, e) and compared with the attitude of ore shoots measured for the 'outcrop area' and 'lake area' respectively (Fig. 5f, g). The attitudes of ore shoots were estimated from Gocad 'curves' digitized on the ore shoots. The attitude of the fold axis affecting the mineralized zones of each domain was calculated from the distribution of poles to median planes created for selected subplanar mineralized zones (Fig. 5d, e) illustrated on Figure 5b and Figure 5c for the 'outcrop area' and 'lake area', respectively. The results for the 'lake area' indicate that the ore shoots are oriented subparallel to the fold axis affecting the mineralized zones (Fig. 5g). The results for the 'outcrop area' are not as conclusive, but still suggest a geometrical relationship between some of the ore shoots and the fold axis affecting the mineralized zones (Fig. 5f). The attitudes of ore shoots and fold axes calculated from Gocad fall within the stereonet domain defined by attitudes of lineations and fold axes collected on the stripped outcrop (Fig. 5h, i).

Alteration and mineralization

This section briefly summarizes the main characteristics of mineralized zones, alteration, and metamorphic assemblages present in the vicinity of the Roberto deposit. The bulk of the mineralized system primarily occurs in a series of subparallel decametre-scale mineralized zones located west of the aluminosilicate-bearing rocks (Fig. 3, 4a). Two principal mineralized zones, referred to as Roberto and East-Roberto, can be distinguished from one another based on their style, mineralogy, gold content, and stratigraphic position. Significant gold values are, however, not restricted to this series of mineralized zones and are widely distributed over the area. The widespread distribution of gold values is associated with a large-scale, protracted hydrothermal system characterized by distal calcium-rich metasomatic replacement zones and veins, and proximal quartz-dravite-arsenopyrite veinlets and quartz±actinolite±diopside± biotite-arsenopyrite-pyrrhotite veins emplaced within quartz-microcline-dravite-biotite-arsenopyrite-pyrrhotite replacement zones hosting the gold mineralization.

Aluminous assemblages

At deposit scale, aluminosilicate-porphyroblast-bearing rocks are located in the hanging wall of the principal mineralized zones and are distributed along two subparallel hectometre-scale zones, the thickness of which varies along strike (Fig. 3) and with depth (Fig. 5a). These aluminous zones are sediment hosted and are dominated by andalusite porphyroblasts (up to 15%), fine-grained microcline, biotite, and quartz. Undeformed muscovite poikiloblasts and amphibole porphyroblasts are also locally present. The andalusite porphyroblasts are commonly entirely pseudomorphed to fibrolite and retrograded to chlorite-sericite-muscovite (Fig. 8a), and locally pseudomorphed to margarite. Within aluminosilicate-bearing rocks, porphyroblasts-rich and porphyroblasts-poor layers are distinguished and are thought to reflect primary compositional layering. Aluminosilicate-bearing metapelite units are common in the region (Bandyayera and Fliszár, 2007); however, it is not certain that the occurrence of aluminosilicate porphyroblasts within some units in the Roberto area reflects only a metamorphosed primary pelitic character. The presence of andalusite close to the ore zones could be related to acid-leached sedimentary rocks that generated aluminosilicate porphyroblasts during metamorphism. The presence of abundant fine-grained microcline and relatively high K_2O content (Table 1) suggests that the aluminosilicate-bearing rocks have been subjected to potassic metasomatism. Although locally anomalous in gold (Table 1), these assemblages are generally barren.

Calcium-rich alteration and assemblages

Discrete calc-silicate-bearing veins and metasomatic replacement bands preferentially occur within the intrados of the deposit-scale fold (Fig. 3) and affect all lithologies but the pegmatite dykes. The mineralogy and textural characteristics of the calcium-rich alteration and/or assemblages change with the nature of the host rock and proximity to the ore zone. In aluminosilicate-bearing host rocks, calc-silicate-bearing assemblages form layers of sericitized and saussuritized feldspar, clinozoisite, biotite porphyroblasts locally retrograded to chlorite and/or prehnite, and minor Ca-rich garnet (Fig. 8b). The calcic nature of these assemblages is portrayed by higher CaO concentrations compared to surrounding aluminosilicate-bearing rocks (Table 1). The calc-silicate-bearing layers are ubiquitously bounded by about 5 cm thick halos where aluminosilicate porphyroblasts did not develop (Fig. 8b).

In other lithologies, such as massive greywacke, the distribution of calcium-rich alteration is fracture controlled and forms 1–5 cm wide replacement bands and selvages (Fig. 8c), some associated with discrete quartz-feldspar veins. The mineralogy of these replacement zones is dominated by actinolite, sericitized and saussuritized feldspar, biotite porphyroblasts locally replaced by chlorite and/or prehnite, pyrrhotite±pyrite, and accessory tourmaline, titanite, clinozoisite, and carbonate. The calcium-rich alteration also occurs as fracture-controlled stockworks and pervasive metasomatic replacement zones (Fig. 8d). The mineralogy of these zones is dominated by actinolite, sericitized and saussuritized feldspar minerals, local microcline, pyrrhotite, and accessory titanite and carbonate. Anomalous gold values (<1 g/t Au) are locally associated with these zones. On the stripped outcrop, pervasive calcium-rich metasomatic replacement is confined to a massive greywacke unit located in the eastern part of the outcrop (Fig. 4a). At deposit scale, such zones are mainly located in the structural hanging wall of the western aluminosilicate-porphyroblast-bearing unit (Fig. 3).

On the large stripped outcrop, the calc-silicate-bearing assemblage changes in proximity to the mineralized zones, where anomalous gold values (<1 g/t Au) are present with coarse diopside (~7mm), microcline, tourmaline, and traces of arsenopyrite (Fig. 8e). In between the two principal mineralized zones, calc-silicate-bearing veins and replacement structures are thicker (up to 50 cm), and locally spatially associated with significant potassic alteration (microcline) and tourmalinization of the host greywacke (Fig. 8f). These wider veins and replacement structures also contain arsenopyrite and are associated with variable gold values (up to 12 g/t Au).

East-Roberto mineralized zone

The East-Roberto mineralized zone (up to 8 g/t Au over 6 m) is located west of the western aluminosilicate-porphyroblast-bearing unit, and is composed of several mineralogical assemblages that have different textural characteristics. The western envelope of the East-Roberto zone comprises hydrothermal breccia with angular millimetre- to centimetre-scale, pinkish-brown fragments of metagreywacke composed of various proportions of microcline, biotite, and saussuritized feldspar that are cut and replaced by quartz-actinolite-diopside veins (Fig. 9a). These hydrothermal breccia units contain anomalous gold values (<1 g/t Au) (Table 1). Closer to the ore zone, the predominant mineralogical assemblage is characterized by a well defined layering composed of centimetre-scale leucocratic quartz-diopside-microcline-arsenopyrite-pyrrhotite veins with local actinolite, saussuritized and/or sericitized feldspar and titanite injected within black tourmaline-rich altered greywacke (Fig. 9b). The intensity of alteration and the layered aspect significantly increases approaching a north-striking, postmineralization slip plane that bounds the eastern side of the mineralized zone, where the different mineralogical assemblages are gradually replaced by quartz, forming irregular centimetre- to metre-wide zones dominated by quartz-rich 'silica flooding' (Fig. 9c). These zones of silica replacement are associated with significant gold values (≥5 g/t Au) and contain various proportions of quartz, microcline, tourmaline, actinolite, diopside, saussuritized feldspar, clinozoisite, and arsenopyrite.

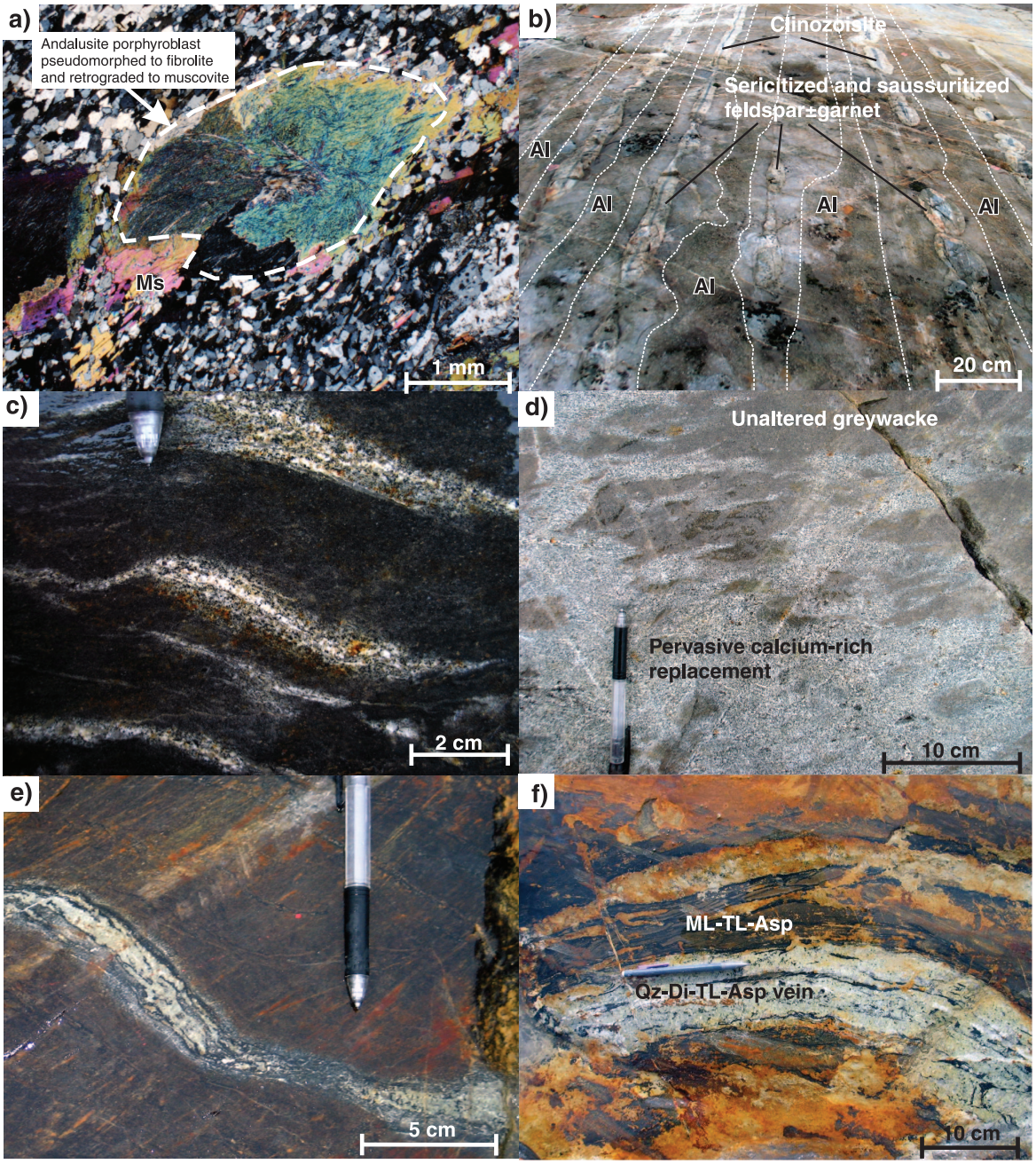

Figure 8. a) Photomicrograph showing an andalusite porphyroblast pseudomorphed to fibrolite and retrograded to muscovite (Ms) (cross-polarized light). 2010-004. **b)** Calc-silicate-bearing replacement bands in aluminosilicate-porphyroblast-bearing (Al) rock. Note the absence of aluminosilicate porphyroblasts in the wall-rock selvages of the replacement bands. 2010-018. **c)** Discrete calcium-rich replacement in massive greywacke. 2010-017. **d)** Pervasive calcium-rich replacement of the host greywacke. 2010-025. **e)** Gold-bearing (<1 g/t Au) quartz-diopside-tourmaline-arsenopyrite vein. 2010-020. **f)** Gold-bearing (up to 12 g/t Au) quartz-diopside-tourmaline-arsenopyrite (Qz-Di-TL-Asp) vein spatially associated with microcline-tourmaline-arsenopyrite (ML-TL-Asp) alteration of the wall rock. 2010-026. All photographs by J.-F. Ravenelle.

Table 1. Geochemical analyses of alteration assemblages associated with the Roberto gold deposit.

Analysis	Au	As	B	SiO_2	Al_2O_3	CaO	MgO	Na_2O	K_2O	Fe_2O_3	MnO	TiO_2	P_2O_5	Cr_2O_3	LOI	Sum	CO_2	S	Sb	Ag	Cu	Zn	Pb	Y	Zr
Detection	5	3	10	0.01	0.01	0.01	0.03	0.02	0.01	0.01	0.01	0.01	0.01	0.01	0.01	0.01	0.01	0.01	5	2	0.5	0.5	2	0.5	0.5
Units	ppb	ppm	ppm	%	%	%	%	%	%	%	%	%	%	%	%	%	%	%	ppm	ppm	ppm	ppm	ppm	ppm	ppm
Aluminous zone																									
D-ELE-05-A	26	52	130	62.5	17.5	2.52	2.9	2.82	3.52	6.03	0.06	0.61	0.15	0.01	1.3	100.1	0.14	0.28	18	<2	45.4	79.7	16	5.3	116
JFR-05-024	187	1540	260	65.7	15.4	1.48	3.00	1.29	5.84	4.2	0.04	0.38	0.12	<0.01	1.9	99.5	0.01	0.43	18	<2	33.9	56.5	30	6	52.9
JFR-05-090	5	21	90	67.1	17.7	1.46	2.65	1.61	3.29	4.24	0.06	0.5	0.11	<0.01	1.7	100.6	0.02	0.27	9	<2	52.1	73.0	57	6	152
JFR-07-304	5	59	180	62.3	17.9	2.28	2.18	2.48	6.28	4.68	0.08	0.59	0.1	0.01	1.06	99.9	0.05	0.26	6	<2	49.8	86.6	32	5.4	96
JFR-07-317F	5	57	140	68.1	14.4	2.03	2.00	2.22	4.6	4.3	0.06	0.51	0.14	0.01	1.25	99.7	0.08	0.38	11	<2	62.4	78.4	33	5.5	106
Average	**46**	**346**	**160**	**65.14**	**16.58**	**1.95**	**2.55**	**2.08**	**4.7**	**4.69**	**0.06**	**0.52**	**0.124**		**1.44**	**99.96**	**0.06**	**0.32**	**12**		**48.7**	**74.8**	**34**	**5.6**	**105**
Standard deviation	80	668	64	2.64	1.58	0.47	0.44	0.63	1.34	0.77	0.01	0.09	0.02		0.35	0.42	0.05	0.08	5		10.4	11.3	15	0.3	35.8
Metasomatic replacement in aluminous zone																									
D-ELE-05-E	5	12	20	68.3	14.6	6	2.11	0.66	1.81	4.04	0.12	0.4	0.12	<0.01	1.95	100.3	0.29	0.12	17	<2	19.4	66.8	7	9.6	101
JFR-07-317J	NA	8	60	67.1	15.9	6.32	1.53	1.56	1.6	2.65	0.09	0.31	0.14	<0.01	2.71	99.9	0.27	0.08	7	<2	17.8	38.6	52	10.4	109
TR-3D	32	41	50	68.1	15	4.88	2.12	0.83	2.62	3.24	0.08	0.39	0.11	<0.01	2.48	99.9	0.21	0.13	<5	<2	20.4	80.2	5	7.9	82.4
Average	**19**	**20**	**43**	**67.83**	**15.17**	**5.73**	**1.92**	**1.02**	**2.01**	**3.31**	**0.1**	**0.37**	**0.12**		**2.38**	**100.03**	**0.26**	**0.11**	**12**		**19.2**	**61.9**	**21**	**9.3**	**97.5**
Standard deviation	19	18	21	0.64	0.67	0.76	0.34	0.48	0.54	0.7	0.02	0.05	0.02		0.39	0.23	0.04	0.03	7		1.31	21.2	27	1.3	13.7
East-Roberto																									
JFR-05-017 (l.m.)	2550	2380	2680	63.9	9.26	7.5	5.64	0.78	3.39	5.39	0.1	0.42	0.14	0.08	0.8	97.6	0.17	0.67	42	<2	56.7	45.2	89	8.9	51.6
JFR-07-325A (h.b.)	116	221	60	74.1	8.84	5.41	3.65	0.53	2.31	3.87	0.08	0.35	0.12	0.04	0.87	100.1	0.03	0.19	50	<2	24.6	49.2	7	7.5	66.8
JFR-07-328A (w.n.c-s)	284	749	570	55.6	16.2	8.07	5.37	0.85	3.16	6.38	0.12	0.63	0.35	0.08	2.46	99.3	<0.01	0.48	20	<2	48.6	71	13	14.2	126
JFR-07-328C (w.c.c-s)	4760	2390	13400	53.5	20.6	5.86	4.62	1.45	0.95	5.73	0.04	0.86	0.35	0.1	1.99	96	<0.01	0.51	43	<2	78.9	24.7	12	13.7	143
JFR-07-344A (w.n.c-s)	130	994	540	56.7	11.6	8.01	7.86	0.76	4.99	7.04	0.14	0.57	0.24	0.19	1.25	99.3	0.01	0.36	31	<2	79.6	65.1	19	11.1	61.3
Average	**1568**	**1347**	**3450**	**60.76**	**13.3**	**6.97**	**5.43**	**0.87**	**2.96**	**5.682**	**0.1**	**0.57**	**0.24**	**0.1**	**1.47**	**98.46**	**0.07**	**0.44**	**37**		**57.7**	**51**	**28**	**11.1**	**89.7**
Standard deviation	2060	988	5654	8.42	5.02	1.25	1.56	0.34	1.48	1.19	0.04	0.2	0.11	0.06	0.73	1.65	0.09	0.18	11		23	18	34	2.9	41.7
Roberto																									
JFR-05-007 (s.w.)	16300*	17200**	5140	62.9	13.1	2.37	2.81	0.79	4.3	6.38	0.05	0.54	0.11	0.03	3	96.6	0.01	2.12	90	<2	56.1	34.5	84	11.9	95.5
JFR-05-011 (s.w.)	7290	11400**	7030	59.7	15.2	1.79	3.46	1.14	3.9	6.79	0.06	0.59	0.19	0.03	2.55	95.5	0.01	2.22	67	<2	67.8	25.8	19	12.5	110
JFR-07-334 (m.w.)	16800*	32100**	3100	61.3	15.1	0.65	1.26	0.84	8.95	6.6	0.01	0.61	0.12	0.04	4.37	99.8	<0.01	2.38	227	<2	47.8	11.1	48	9.3	103
JFR-07-346a (m.w.)	21800*	27700**	3330	67.6	13.3	3.18	1.45	1.12	2.69	5.23	0.03	0.53	0.1	0.03	3.73	98.9	<0.01	1.9	189	<2	31.3	12.1	11	7.2	94.3
JFR-07-347a (m.w.)	13800*	26000**	3240	65	13.8	3.84	1.56	0.89	3.88	5.34	0.02	0.52	0.13	0.04	3.48	98.5	<0.01	1.88	135	<2	30.2	10.8	30	8.9	85.5
Average	**15050**	**21600**	**4190**	**63.95**	**13.45**	**3.11**	**2.19**	**0.84**	**4.09**	**5.86**	**0.04**	**0.53**	**0.12**	**0.04**	**3.24**	**97.55**	**0.01**	**2**	**112**		**43.2**	**22.7**	**57**	**10.4**	**90.5**
Standard deviation	5288	8397	1706	3.1	0.99	1.24	0.97	0.16	2.43	0.73	0.02	0.04	0.04	0.01	0.7	1.76	0	0.21	66		16.2	10.8	29	2.2	9.28

* = Detection limit 30 ppb

** = Detection limit 30 ppm

l.m. = layered material

h.b. = hydrothermal breccia

w.n.c-s = greywacke near calc-silicate-bearing vein

w.c.c-s = greywacke in contact with calc-silicate-bearing vein

s.w. = mineralized stockwork (greywacke+quartz-tourmaline-arsenopyrite veinlets)

m.w. = mineralized greywacke in stockwork (without veins or veinlets)

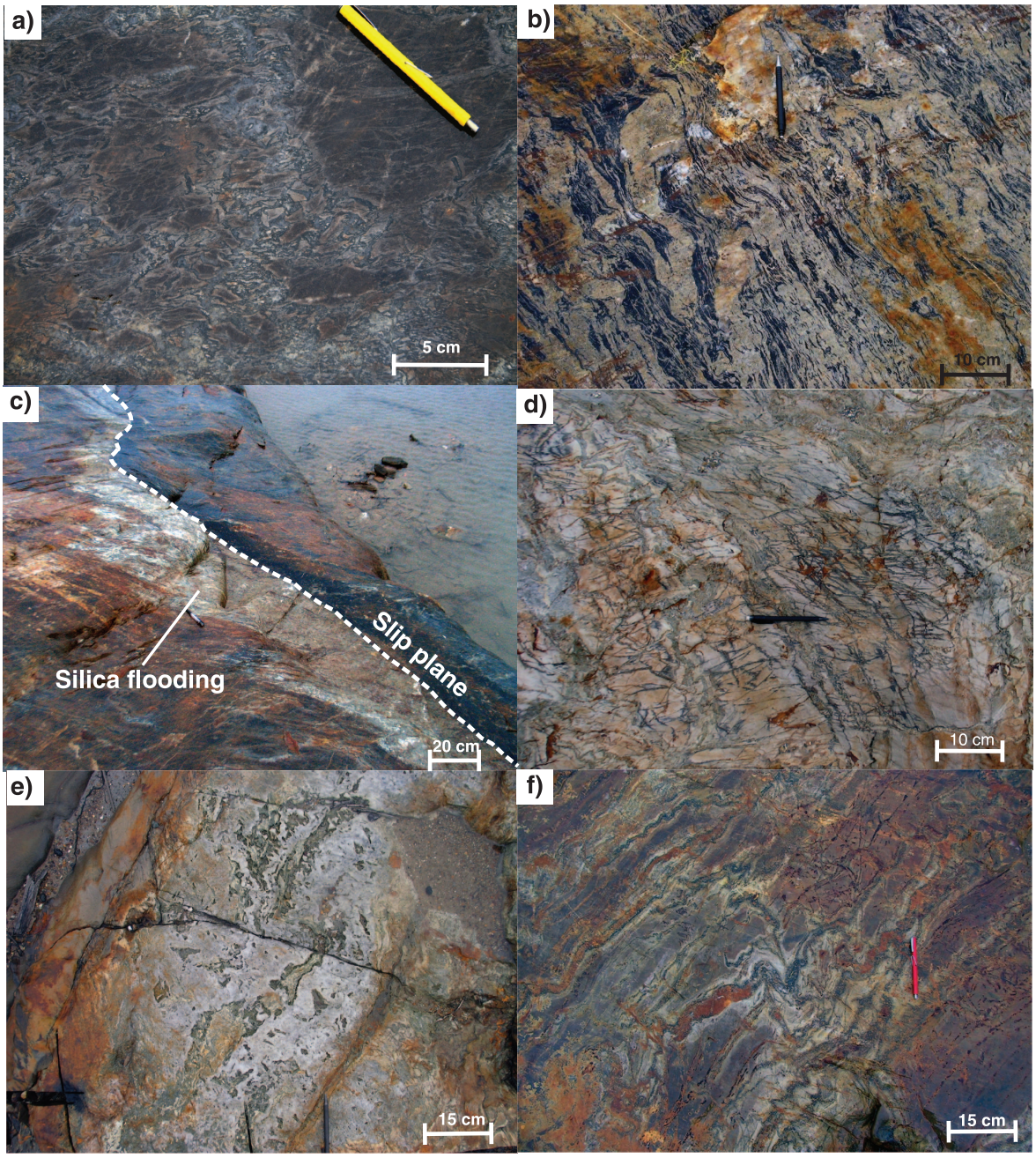

Figure 9. a) Hydrothermal breccia of the East-Roberto zone. Photograph by B. Dubé. 2010-014. **b)** Highly deformed layering within the East-Roberto zone. Note the presence of isoclinal folds. Photograph by J.-F. Ravenelle. 2010-009. **c)** Slip plane that bounds the eastern border of the East-Roberto zone characterized by a zone of silica flooding (white area). Photograph by J.-F. Ravenelle. 2010-011. **d)** Mineralized stockwork of the Roberto zone. Photograph by J.-F. Ravenelle. 2010-022. **e)** Metre-scale quartz-actinolite-arsenopyrite-pyrrhotite vein that bounds the western border of the Roberto zone over several tens of metres. Photograph by J.-F. Ravenelle. 2010-028. **f)** High-grade part (>20 g/t Au) of the Roberto mineralized stockwork. Photograph by B. Dubé. 2010-016.

In the northern portion of the stripped outcrop, the East-Roberto mineralized zone contains less diopside, is more silicified and higher grade (~12 g/t Au over 7 m), and is locally highly strained. North of the stripped outcrop, drill-core data shows that the continuation of the East-Roberto zone is also more silicified and higher grade. The heterogeneous distribution of alteration assemblages which include calc-silicate-bearing assemblages, potassic hydrothermal breccia units, silica flooding, and abundant arsenopyrite and tourmaline, respectively translates into high concentrations of CaO, K_2O, SiO_2, As, and B in geochemical analyses (Table 1).

Roberto mineralized zone

The Roberto mineralized zone (typically averaging 12 g/t Au over 10 m) represents the core of the auriferous hydrothermal system and the most important mineralized zone of the deposit. It consists of a stockwork of quartz± actinolite±diopside±phlogopite-biotite-arsenopyrite-pyrrhotite veins and quartz-dravite-arsenopyrite veinlets contained within highly altered sedimentary rocks composed of quartz-microcline-dravite-phlogopite-biotite (locally replaced by chlorite)-saussuritized feldspar-arsenopyrite-pyrrhotite and accessory clinozoisite and titanite (Fig. 9d). This mineralized stockwork is primarily hosted by thinly bedded (2–8 cm thick beds) greywacke units bounded by less-altered massive greywacke. The quartz±actinolite± diopside±phlogopite-biotite-arsenopyrite-pyrrhotite veins of the stockwork are generally centimetre- to decimetre-scale thick and locally contain visible gold. Such a quartz vein is 30–50 cm thick (Fig. 9e) and bounds the western edge of the Roberto zone over several tens of metres. High-grade regions of the mineralized stockwork (>20 g/t Au) are associated with high proportions of fine-grained microcline and disseminated tourmaline (dravite) and arsenopyrite, which typically give a deep pinkish-brown colour to the rock (Fig. 9f) and make high-grade regions easily recognizable at surface. In drill cores, the stockwork style of mineralization generally coincides with a well defined layering characterized by transposed quartz-tourmaline veinlets and microcline-rich bands (Fig. 10). Reflected-light microscopy indicates the

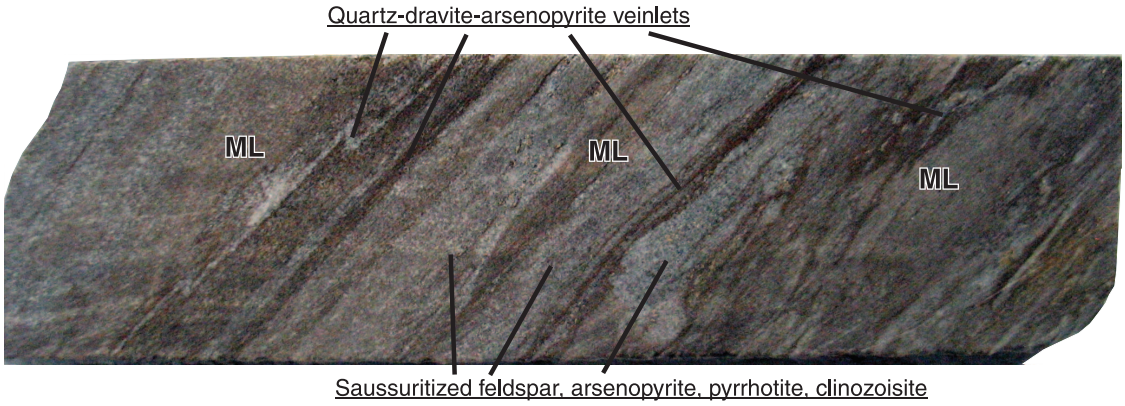

Figure 10. Drill core sample of Roberto's mineralized stockwork showing well defined layering. (ML = microcline (±arsenopyrite-pyrrhotite)). Photograph by J.-F. Ravenelle. 2010-019.

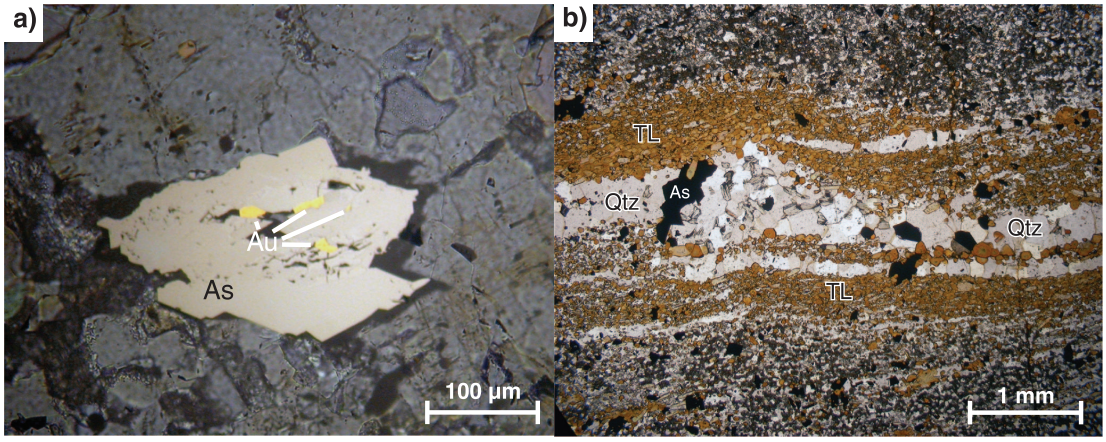

Figure 11. a) Visible gold contained within an arsenopyrite crystal (As) (reflected light). 2010-031. **b)** Arsenopyrite crystals (As) contained within a quartz (Qtz) tourmaline (TL) veinlet of the Roberto stockwork (cross-polarized light). 2010-024. Both photographs by J.-F. Ravenelle.

presence of gold within arsenopyrite crystals (Fig. 11a) and locally within pyrrhotite crystals, which further suggests that a genetic relationship exists between gold, arsenopyrite, and quartz-tourmaline veinlets that locally host the arsenopyrite and pyrrhotite (Fig. 11b). This relationship is also portrayed in geochemical analyses that clearly show that elevated gold values are associated with high As, B, and S content. Gold values are also associated with moderate Sb concentrations, but not with significant base-metal concentrations (Table 1). The occurrence of löllingite (a mineral typically found in high-temperature gold deposits (e.g. Mueller and Groves, 1991)) among arsenopyrite crystals has also been indicated by X-ray diffraction and microprobe analyses.

Other mineralized zones

Auriferous zones and sporadic gold values are locally present between the Roberto and East-Roberto zones and elsewhere in the footwall and hanging wall of the mineralized envelope. In general, these mineralized zones are composed of various proportions of calc-silicate minerals, microcline, tourmaline, arsenopyrite, and pyrrhotite; but lack the well developed mineralized stockwork of Roberto or intense layering of East-Roberto zones. On the stripped outcrop, the most significant of such mineralized zones is the Mid-Roberto zone, which branches out from the Roberto zone and almost joins the East-Roberto zone (Fig. 4a). Some mineralized zones are hosted by other lithological units including paragneiss units, biotite schist units, and conglomerate units, which give them specific characteristics. In the northern limb of the deposit-scale fold, mineralized zones are locally associated with metre-scale quartz-arsenopyrite veins that locally contain visible gold (e.g. on trench 08-10, Fig. 12). Mineralized zones hosted within paragneiss sequences were intersected through drilling and appear to have been subjected to a higher degree of metamorphism and hence possess different attributes. For example, gold mineralization in an impressive mineralized zone (60 g/t Au over 30 m) intersected in the deeper levels of the deposit (about 1.2 km depth) is associated with quartz-feldspar-arsenopyrite-pyrrhotite veins that contain visible gold, but where calc-silicate-bearing assemblages or microcline are absent. Importantly, these auriferous quartz-feldspar-arsenopyrite-pyrrhotite veins locally gradually evolve into pegmatitic material, which may suggest that they are genetically related to an episode of pegmatite magmatism. Other mineralized zones in paragneiss are characterized by deformed quartz-arsenopyrite-pyrrhotite veins hosted within recrystallized saccharoidal quartz-feldspar-phlogopite-biotite-sericite asemblages with pyrrhotite and fine arsenopyrite and löllingite (Fig. 13). Local bright green mica (Cr-rich muscovite) was also documented in such zones.

Relative chronology of hydrothermal system

The stripped outcrop provided the opportunity to document crosscutting relationships (and hence relative chronology) between different elements of the hydrothermal

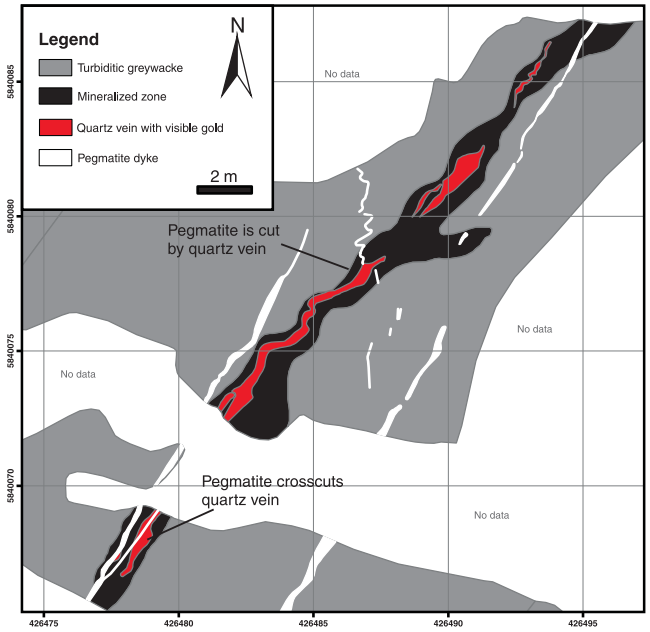

Figure 12. Geological map of trench 08-10 showing crosscutting relationships between pegmatite dykes and an auriferous quartz vein associated with a mineralized zone. The folded pegmatite dyke cut by the auriferous quartz vein in the centre portion of the map represents the only example of a preore pegmatite dyke found in the vicinity of the Roberto deposit. Co-ordinates are in UTM NAD 83.

system. Calc-silicate-bearing veins and mineralized zones are cut by a set of extensional decimetre- to metre-scale quartz-feldspar±tourmaline±arsenopyrite±pyrrhotite veins and veinlets (Fig. 14a, 4a) that locally generated tourmaline-rich veinlets or replacement invading the main S_2 fabric, forming irregular black selvages in the wall rock. These veins generally contain anomalous gold values (<1 g/t Au) and locally show pegmatitic textures.

Pegmatite dykes ranging from a few centimetres to several metres in thickness are widely distributed on the stripped outcrop (Fig. 4a). They are locally auriferous and contain various proportions of arsenopyrite, pyrrhotite, and tourmaline crystals oriented perpendicular to dyke walls. They also locally generated tourmaline-rich impregnation in the wall rock. Crosscutting relationships indicate that these dykes postdate the mineralized zones, the calc-silicate-bearing veins and replacement bands, and the quartz-feldspar vein set. A pre- to synore pegmatite dyke, however, was found on trench 08-10 (located about 400 m to the north of the large stripped outcrop). There, an approximately 40 cm wide quartz vein containing visible gold and arsenopyrite crosscuts a folded pegmatite dyke with an aplitic core (Fig. 12). The reverse crosscutting relationship is exposed a few metres away where a similar dyke cuts across the auriferous quartz vein (Fig. 12), hence suggesting that these pegmatite dykes are contemporaneous with the auriferous high-grade quartz vein.

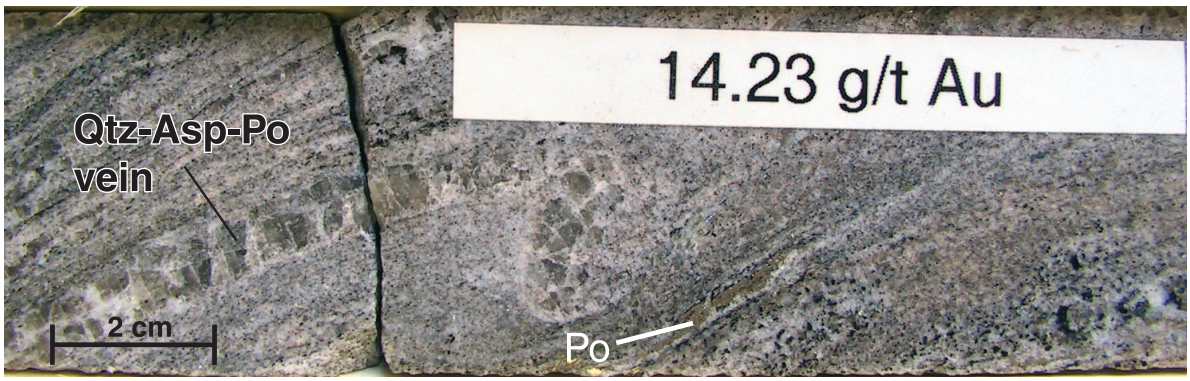

Figure 13. Drill core sample of mineralized zone hosted in paragneiss showing recrystallization of the mineralized assemblage (saccharoidal texture), and folding of mineralized veins and main foliation; Qtz = quartz, Asp = arsenopyrite, Po = pyrrhotite. Photograph by B. Dubé. 2010-030.

Description of chronology between deformation, alteration, and mineralization

The discrete calc-silicate-bearing veins and replacement bands have been deformed by D_2. In the aluminous assemblages, the calc-silicate-bearing bands are both concordant and discordant to bedding planes, and are commonly boudinaged (Fig. 8b) and folded by F_2 folds (Fig. 14b). At one specific location, however, metasomatic material within a replacement band is preferentially developed along S_2 foliation planes (Fig. 14c). Discrete calc-silicate-bearing veins and replacement structures in other lithological units (e.g. massive or bedded turbidite units) are commonly boudinaged and are generally oriented parallel to bedding and S_2 planes.

Although the envelope of the East-Roberto zone has a simple geometry (Fig. 4a), the presence of isoclinal folds and intense transposition in mineralized layers and quartz veins (Fig. 9b, 14e) indicates that the zone is internally highly strained. The axial planes of such folds, interpreted as F_2 folds, are dragged along the north-striking slip plane that bounds the East-Roberto zone (Fig. 9c).

Within Roberto's mineralized stockwork, tourmaline veinlets have multiple orientations; however, they are commonly emplaced along bedding and S_2 planes (Fig. 14d). Where emplaced along bedding planes, tourmaline veinlets are commonly crenulated by S_2. Where emplaced along S_2 planes, they are interpreted to fill pressure-solution cleavage planes. Calc-silicate-bearing quartz-biotite veins of the mineralized stockwork are generally emplaced along bedding planes, are commonly boudinaged, and are locally folded by F_2 folds (Fig. 15a). The mineralized stockwork is in part preferentially developed on the short limb of metre-scale F_2 folds (Fig. 16).

Petrographic analysis of calc-silicate-bearing veins and replacement bands and mineralized material indicates that even though they have recorded mesoscopic D_2 deformation, a large proportion of minerals hosted within these structures does not show microstructural evidence of S_2 or S_3. For example, undeformed euhedral actinolite and large biotite porphyroblasts confined to metasomatic material and mineralized zones are unoriented and appear post-tectonic (Fig. 15b). This suggests that an episode of static recrystallization has outlasted D_2 and D_3. In addition, some of these minerals are commonly replaced by lower-greenschist- and locally prehnite-pumpellyite-facies assemblages (e.g. biotite replaced by chlorite and/or prehnite), which suggests that they have been subjected to significant retrograde metamorphism.

The quartz-feldspar±tourmaline±arsenopyrite±pyrrhotite vein set that postdates calc-silicate-bearing veins and mineralized zones is commonly boudinaged and is widely distributed on the stripped outcrop (Fig. 4a) where it is emplaced as en echelon or sheeted vein sets (Fig. 15c). Some vein sets locally crosscut the north-striking slip plane that bounds the East-Roberto zone (Fig. 4a). As mentioned above, tourmaline is locally present as impregnation in the wall rock of these veins, preferentially along S_2 foliation planes (Fig. 15d).

There appears to be at least two generations of pegmatite dykes. The first generation is locally boudinaged (e.g. Fig. 15e) and/or folded by F_2 folds (e.g. Fig. 4a, circled number 1; Fig. 12), while the second generation is not affected by D_2 structures. An example of a post-D_2 pegmatite dyke is present on the large stripped outcrop where it crosscuts the north-striking slip plane that transects the East-Roberto zone (Fig. 15f; 4a, circled number 2), which as described above, drags the S_2 fabric and F_2 axial planes. Finally, all hydrothermal structures, including the calc-silicate-bearing veins and replacement structures, the mineralized zones, the quartz-feldspar veins, and the two generations of pegmatite dykes, are deformed by decimetre- to metre-scale F_3 folds.

GEOCHRONOLOGY

Geochronological work was conducted at the GSC laboratory in order to define the age of the host rocks and the relative timing between turbiditic greywacke that host the

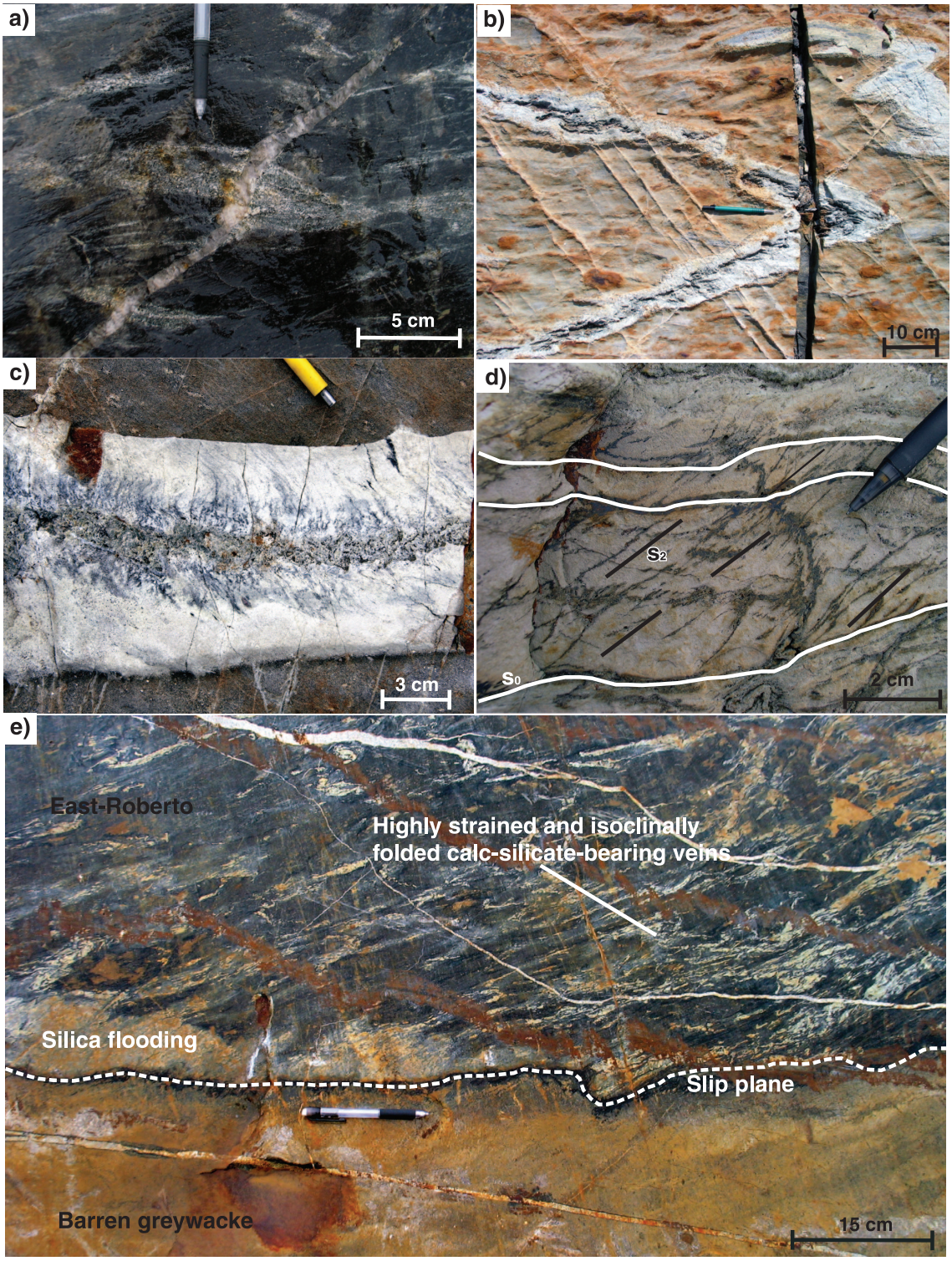

Figure 14. a) Quartz-feldspar±tourmaline±pyrrhotite vein crosscutting calc-silicate-bearing replacement bands. Photograph by J.-F. Ravenelle. 2010-032. **b)** F_2 folds affecting calc-silicate-bearing replacement bands in aluminosilicate-bearing rocks. Photograph by J.-F. Ravenelle. 2010-003. **c)** Preferential injection of material along the S_2 fabric within a replacement band. Photograph by B. Dubé. 2010-007. **d)** tourmaline veinlets emplaced along bedding and S_2 foliation planes within the mineralized Roberto stockwork. Photograph by J.-F. Ravenelle. 2010-033. **e)** Internal deformation within the East-Roberto zone. Photograph by J.-F. Ravenelle. 2010-008.

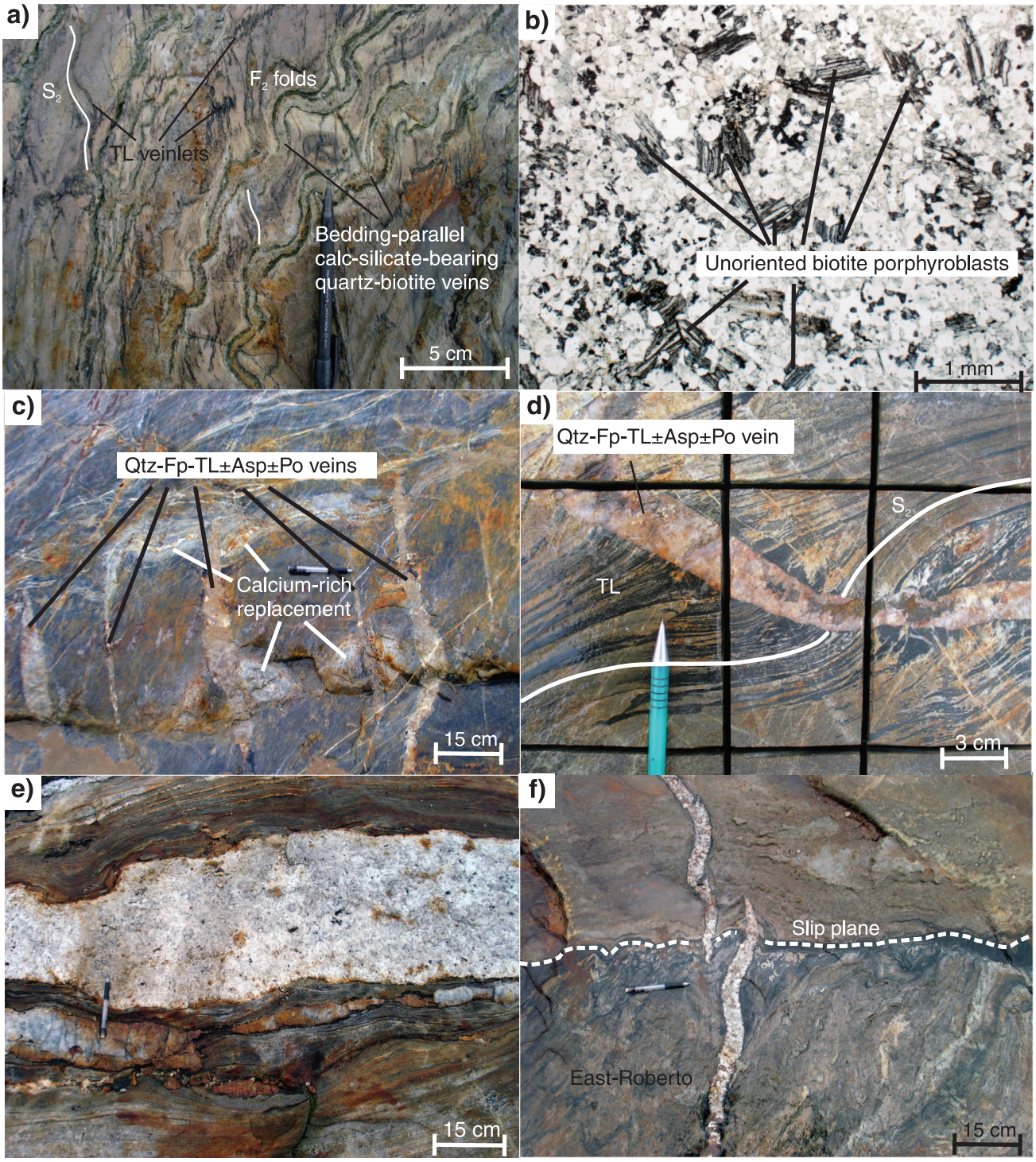

Figure 15. a) Bedding-parallel calc-silicate-bearing quartz-biotite veins (associated with microcline, saussuritized feldspar, tourmaline (TL), and arsenopyrite) folded by F_2 folds in Roberto's mineralized stockwork. 2010-010. **b)** Photomicrograph showing unoriented biotite porphyroblasts (natural light). 2010-005. **c)** Sheeted quartz-feldspar-tourmaline±arsenopyrite±pyrrhotite (Qtz-Fp-TL±Asp±Po) veins crosscutting calc-silicate-bearing replacement bands. 2010-012. **d)** Quartz-feldspar-tourmaline±arsenopyrite±pyrrhotite vein injecting tourmaline in the wall rock along S_2 foliation planes. 2010-021. **e)** Boudinaged pegmatite dyke in paragneiss (dated at ca. 2616 Ma). 2010-015. **f)** Pegmatite dykes crosscutting the slip plane that transects the East-Roberto zone (location of photograph = circled number 2 on Fig. 4a). 2010-027. All photographs by J.-F. Ravenelle.

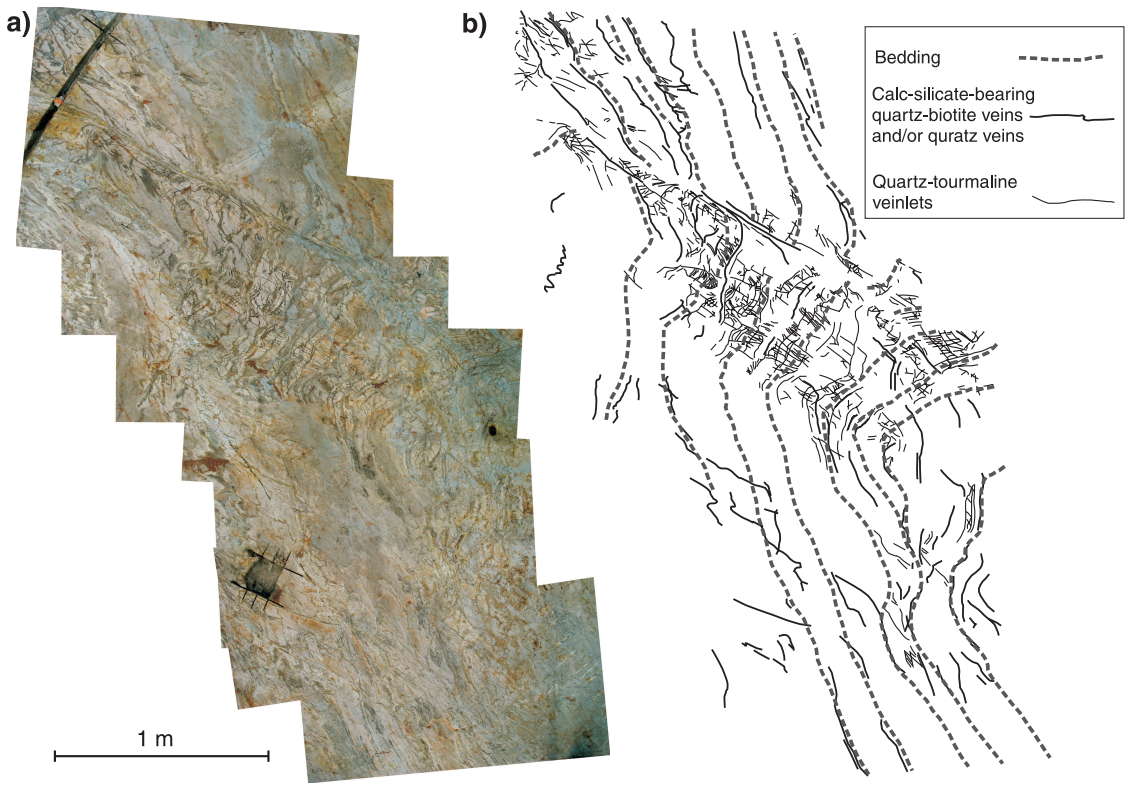

Figure 16. a) Photograph showing a part of Roberto's mineralized stockwork where the stockwork is preferentially developed on the short limb of a metre-scale F_2 Z-fold. 2010-029. Photograph by J.-F. Ravenelle. **b)** Interpreted drawing of the photograph in Figure 16a showing the details of the mineralized stockwork.

deposit, regional conglomerate sequences, the mineralized phase of the Ell Lake diorite, and pegmatitic magmatism hosted within paragneiss units. The mineralized phase of the Ell Lake diorite was previously dated by J. David (GEOTOP) for Virginia Gold Mines, at 2705 ± 1.9 Ma (J. David, unpub. report for Virginia Gold Mines Inc., 2005). In this study, U-Pb high precision geochronology was performed by Sensitive High Resolution Ion Micro Probe (SHRIMP) and thermal-ionization mass spectrometry (TIMS) to constrain the deposition age of the regional conglomerate and of the greywacke that hosts the Roberto zone. The maximum age of the conglomerate (age of the youngest zircon present within the sample) is 2702 ± 3 Ma. The maximum age of the greywacke hosting the Roberto zone is 2675 ± 6 Ma. A pegmatite dyke emplaced within paragneissic units (*see* Fig. 2 for location) and that has been boudinaged by D_2 (Fig. 15e) is dated at ca. 2616 Ma.

DISCUSSION

Tectonic setting

A schematic stratigraphic column with age constraints for the Éléonore property is presented on Figure 17. The oldest lithological units are represented by mafic volcanic rocks that are intruded by dioritic to tonalitic phases of the Opinaca pluton dated between 2708.9 ± 0.9 Ma and 2703.5 ± 2.8 Ma (Bandyayera and Fliszár, 2007). The mafic volcanic rocks are conformably overlain by intermediate tuff units dated at 2704 ± 1 Ma (Bandyayera and Fliszár, 2007), and unconformably overlain by conglomerate sequences dated at less than 2702 ± 3 Ma. The zircon population within conglomerate shows a peak at 2707 Ma, corresponding within errors to the age of the Ell Lake intrusion, which suggests that the majority of diorite blocks contained within conglomerate sequences originate from the Ell Lake intrusion or other coeval intrusions, and that the conglomerate units are deposited stratigraphically above the Ell Lake intrusion. It was locally observed, however, that the Ell Lake intrusion cut through the conglomerate sequences. Similar conflicting timing relationships have been documented in other regions, for example in the Kirkland Lake district of the Abitibi Subprovince, where sedimentary rocks of the Timiskaming Group are locally

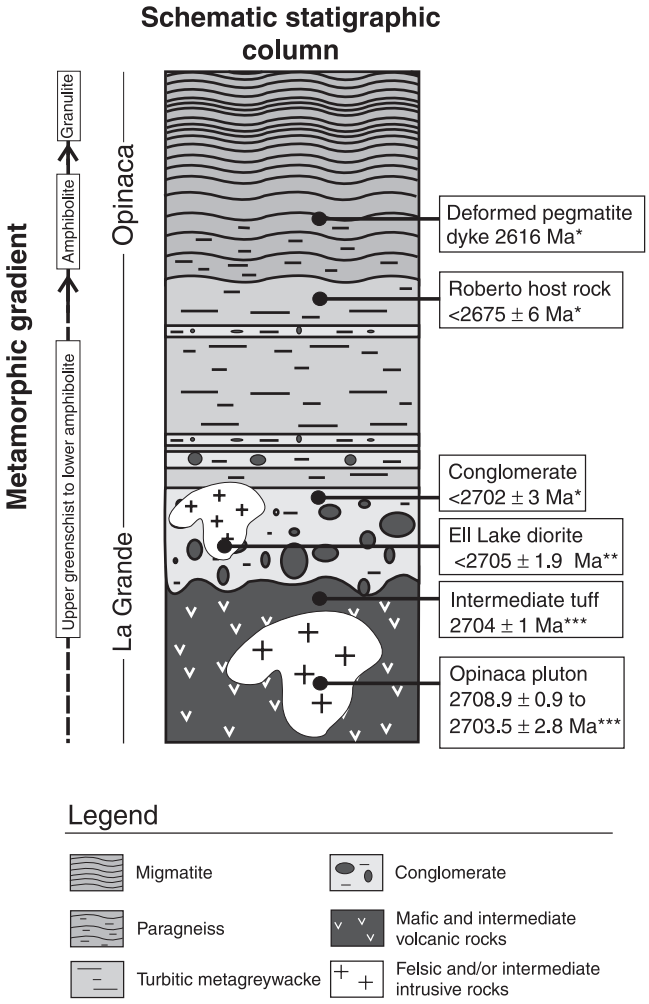

Figure 17. Schematic stratigraphic column illustrating the relative chronology of stratigraphic and intrusive phases (* this study, ** J. David (unpub. report for Virginia Mines Inc., 2005), *** Bandyayera and Fliszár (2007)).

in erosional contact with syenite stocks (e.g. Robert, 2001) in spite of the fact that most syenite intrusions cut the sedimentary rocks (e.g. Ispolatov et al., 2008). The conflicting timing relationships suggest that crystallization of the Ell Lake intrusion occurred during the tectonic uplift that led to the formation of the conglomerate units. This scenario could imply that the tectonic uplift that potentially marked the onset of D_1 occurred ca. 2705 Ma, which agrees with the estimated age bracket of 2710–2697 Ma established by Moukhsil et al. (2003) for D_1. The fact that the main deformational event, here interpreted as D_2, affected a pegmatite dyke dated at 2616 Ma within paragneiss units of the Opinaca Subprovince (Fig. 15e) indicates that D_2 was a protracted event still active at ca. 2616 Ma, and therefore represents a much younger tectonic and metamorphic event compared to other events described in the Superior Province (e.g. Percival, 2007).

The tectonic setting under which the large migmatite and granulite terrain of the Opinaca Subprovince was generated is not well defined. The formation of migmatite and granulite terrains requires high heat flow (Bohlen, 1991), which can be generated in various tectonic settings including convergent plate margins (e.g. Johnson et al., 2003), continental extensional settings (e.g. Kruckenberg et al., 2008), and back-arc basin settings (e.g. Jones and Brown, 1990). Similarities between the Opinaca Subprovince and the English River Subprovince of Ontario in terms of metamorphic grade and nature of protolith could suggest that the Opinaca Subprovince is the lateral continuity of the English River Subprovince, which is thought to represent a synorogenic flysch basin based on the turbiditic nature of its greywacke and the span of sediment deposition (2705 to 2698 Ma), which occurred after arc activity and close to the time of collisional orogeny (Percival, 2007). A comparative geochemical study also indicates that the geochemistry of Opinaca Subprovince paragneiss is similar to the geochemistry of paragneiss found in the Quetico Subprovince (Doyon, 2004), which combined with other aspects, might indicate that the two subprovinces had similar source material (Moukhsil et al., 2003). The Quetico Subprovince is thought to represent an accretionary prism (Percival, 1989) associated with a continental arc (Moukhsil et al., 2003). Alternatively, D. Bandyayera and others (D. Bandyayera, C. Maurice, P. Rhéaume, and P. Keating, work presented at Quebec Exploration Conference, Québec, Quebec, November 25, 2008) proposed a model involving continental extension to explain the migmatization of the Opinaca Subprovince.

Even though the tectonic setting of the Roberto deposit is not well defined, its regional stratigraphy characterized by the presence of ultramafic and mafic volcanic rocks unconformably overlain by coarse clastic rocks, the presence of high-strain zones and magmatic activity in the area, and its proximity with the contact between two subprovinces, indicate that the Roberto deposit possesses some of the important attributes of well known gold-rich greenstone belts as described by Robert et al. (2005) and Dubé and Gosselin (2007).

Distribution of the S_2 fabric on the stripped outcrop

The complex distribution of the S_2 fabric mapped on the large stripped outcrop (Fig. 4a) might be attributed to the interplay between at least two factors: folding of S_2 (initially oriented east-west) during D_3, and dragging and reorientation of S_2 caused by local slip along lithological or fault contacts during D_2 and/or D_3. Field observations suggest that slip along some of these lithological or fault contacts can be constrained to have occurred either late during D_2 or early during D_3. First, the fact that a pegmatite dyke crosscuts the slip plane near the East-Roberto zone (and is hence younger) (Fig. 15f), but is itself folded by F_3 folds (Fig. 4a, circled number 2) strongly suggests that movement along that slip plane occurred before folding of the pegmatite dyke (i.e. before D_3 or early in D_3). Second, the fact that the same slip

plane drags previously formed D_2 structures (S_2 fabric and F_2 axial planes) (Fig. 9c, 4a) strongly suggests that movement along the slip plane occurred after D_2 or late in D_2. The combination of these observations indicates that movement along the slip plane occurred either late during D_2 or early during D_3.

Geometry of deposit-scale fold

In detail, the map pattern and 3-D geometry of lithological units around the Roberto deposit are complex (Fig. 3, 5). This complexity is in part related to significant changes in the thickness of aluminosilicate-bearing sequences (Fig. 3, 5). The presence of high-strain zones near the most significant changes in thickness could suggest that this distribution is structurally controlled and that domains with different structural affinities were juxtaposed through vertical movement along such high-strain zones. On the other hand, such thickness changes might alternatively be attributed to 1) local variations in the intensity and nature of the hydrothermal alteration which could have locally precluded the formation of aluminosilicate (*see* 'Relative timing between calcium-rich alteration and metamorphic peak' section), and 2) the possibility that the aluminosilicate porphyroblasts represent an alteration product the distribution of which is discordant to lithological units. These different scenarios are not exclusive of one another and a combination of factors might explain the observed change in thickness.

The geometric complexity also relates to the discontinuous distribution of certain lithological units (e.g. conglomerate, arenitic wacke, biotite schist), which suggests that these units were significantly boudinaged during deformation or that they had a primary lenticular distribution. The presence of high-strain zones near significant discontinuities in these lithological units could, however, suggest that, as for the aluminosilicate-bearing rocks, their initial geometry might have been modified by high-strain zones.

The map pattern also shows a relatively complex deposit-scale symmetrical repetition of lithological units (conglomerate–aluminous rocks–arenitic wacke) (Fig. 3, circled numbers 1, 2, 3). Although such a repetition might simply illustrate primary depositional repetitions and hence be purely circumstantial, such a repetition might, on the other hand, indicate that these rocks were isoclinally folded prior to the formation of the kilometre-scale F_2 fold; however, evidence of a deformation predating D_2 is cryptic in this sector. An alternative hypothetical explanation is that the map pattern of Figure 3 represents a slice through a sheath-fold geometry (analogous to the second slice of Fig. 7). Such a sheath fold might have been generated through movement along high-strain zones that transposed already formed folds parallel to their stretching direction.

Timing between gold mineralization and deformational events

One of the most important characteristics of the deposit is that the alteration and mineralization is deformed and is primarily confined to a deposit-scale F_2 fold hinge. This distribution could result from two genetic scenarios: 1) gold mineralization occurred before folding, and was subsequently preferentially preserved in the hinge area as opposed to being destroyed and remobilized on highly stretched limbs; or 2) gold mineralization occurred early during folding and folding mechanisms played an essential role in controlling sites of gold mineralization as it is for many turbidite-hosted gold deposits (e.g. Ryan and Smith, 1998). Distinction between the two scenarios relies on field observations that illustrate the timing between gold-mineralized structures and deformational features. As described earlier, mineralized zones and associated alteration have recorded a significant amount of strain and metamorphism associated with D_2, which suggests that gold mineralization has been introduced either before D_2 or early during D_2.

The fact that the mineralized stockwork of the Roberto zone is locally preferentially developed on the short limb of metre-scale F_2 folds (Fig. 16) suggests that folding mechanisms potentially controlled (at least locally) sites of stockwork formation and hence gold mineralization. This interpretation is also compatible with (but not proven by) the fact that the distribution of tourmaline veinlets within the Roberto stockwork is in part controlled by S_2 (Fig. 14d, 15a) through the generation of a pressure-solution cleavage. The fact that high-grade ore shoots are subparallel to deposit-scale fold axes (Fig. 5) does not prove or disprove any of the scenarios, as gold mineralization generated before folding would likely be remobilized and transposed parallel to the fold axis and stretching direction, and gold mineralization generated during folding would also likely be prone to bear geometrical relationships with fold axes. Regardless of which of the scenarios is applicable, it should be noted that examples where gold mineralization is spatially associated with F_2 folds are found elsewhere in the region (e.g. Auclair prospect (Chapdelaine and Huot, 1997) and Clearwater prospect (Cadieux, 2000; Tremblay, 2006)) and that targeting regions affected by F_2 folds, especially near the contact between the Opinaca and La Grande subprovinces, might prove to be a valuable empirical prospecting criteria.

Hydrothermal relationship between gold mineralization and calcium-rich alteration

A hydrothermal link between mineralized zones and calcium-rich alteration is supported by the combination of numerous observations which include: 1) calcium-rich alteration is mainly distributed within the deposit-scale fold area that affects the mineralized zones and thus globally spatially related to the mineralized zones; 2) auriferous calcium-rich veins are present in the Roberto zone and represent one of

the principal constituents of the East-Roberto zone; 3) calc-silicate-bearing veins are locally associated with potassic alteration and tourmalinization of their host greywacke, which represent important alteration characteristics of the Roberto zone; 4) calc-silicate-bearing veins and replacement structures are locally auriferous and contain arsenopyrite; 5) the timing of calcium-rich alteration and mineralized zones with respect to the D_2 deformation appears to be the same (pre- or early-D_2).

Relative timing between calcium-rich alteration and metamorphic peak

The fact that aluminosilicate porphyroblasts are typically not developed around calc-silicate-bearing bands of the aluminous zones (Fig. 8b) might indicate that calcium-rich replacement occurred before the formation of porphyroblasts and hence before the peak of metamorphism. The proposed scenario is that by increasing the concentration of certain elements (e.g. CaO) in the host rock, metasomatic replacement decreased the relative proportion of aluminum which subsequently precluded aluminosilicate formation during prograde metamorphism of the metasomatized regions. This interpretation agrees with the fact that the calc-silicate-bearing veins and replacement bands have recorded a significant amount of strain related to D_2, and that high-grade metamorphism is at least locally superposed on pre-existing ore (e.g. Fig. 13). As previously mentioned, variations in the thickness of aluminosilicate-bearing sequences (Fig. 3, 5) might accordingly be explained by variations in the intensity of the calcium-rich alteration. Although presence of metasomatic material injected along S_2 planes within a replacement band (Fig. 14c) would suggest that a part of the metasomatic replacement was introduced as the S_2 fabric was forming, its significance is questionable since it has only been documented at one specific location.

Nature of hydrothermal system

In terms of mineralogy, the calcium-rich alteration characterized by the presence of clinozoisite, diopside, and actinolite in association with microcline, tourmaline, arsenopyrite, and pyrrhotite shares analogies with the mineralogical assemblage that characterizes the gold-skarn hydrothermal signature of amphibolite-facies gold deposits (e.g. Mueller and Groves, 1991) such as those found in hypozonal orogenic settings.

At this stage, three scenarios are considered for the origin of the mineralized system: a pre- or early-stage-D_2 auriferous hydrothermal system subsequently deformed and metamorphosed, an orogenic hydrothermal system driven by prograde metamorphic reactions associated with migmatization of the Opinaca Subprovince, or a combination of both. Geochronological data from the Ell Lake diorite and Roberto's host rocks refutes the hypothesis that Roberto's hydrothermal system is genetically related to the Ell Lake intrusion; however, the potential input from magmatic fluids should not be discarded, as indicated by the presence of feldspar porphyry intrusions in the vicinity of the deposit (Fig. 3), and the presence of pegmatite dykes that locally appear to be contemporaneous with mineralized zones (Fig. 12). It is thus plausible that a generation of pegmatite is associated with a part of the mineralization or is associated with a second gold event. On the other hand, there is evidence that some auriferous pegmatite dykes clearly crosscut the mineralized zones and postdate D_2, suggesting that the presence of gold in some pegmatite bodies is in part related to a contamination process that results from emplacement of dykes through mineralized material.

SUMMARY AND CONCLUSIONS

Gold mineralization at the Roberto deposit is mainly hosted by turbiditic greywacke and paragneiss units, and primarily occurs in a series of subparallel decametre-scale-wide mineralized zones spatially associated with a kilometre-scale F_2 fold. The mineralization is related to a protracted hydrothermal system characterized by distal calcium-rich metasomatic replacement zones and veins, and gold-bearing quartz-dravite-arsenopyrite veinlets and quartz±actinolite±diopside±biotite-arsenopyrite-pyrrhotite veins hosted within quartz-microcline-dravite-biotite-arsenopyrite-pyrrhotite auriferous replacement zones. While most of the alteration and mineralized zones are deformed by D_2, other parts appear to be controlled by D_2 structures. Gold mineralization is thus interpreted as being pre- or early-D_2. In descriptive terms, the Roberto deposit shares analogies with disseminated-stockwork style of gold mineralization present in the Superior and Yilgarn cratons as described by Poulsen et al. (2000) and Robert et al. (2005). The fact that aluminosilicate porphyroblasts did not develop in the wall-rock selvages of calc-silicate-bearing replacement bands suggests that the replacement occurred before the metamorphic peak. As the calcium-rich alteration appears to be genetically related to gold mineralization, this interpretation suggests that gold mineralization was also introduced before the metamorphic peak. A premetamorphic peak introduction of gold mineralization is compatible with the fact that high-grade metamorphism is locally superimposed on pre-existing ore, and could further suggest that calc-silicate-bearing veins and replacement represent metamorphosed equivalents of quartz-carbonate veins and carbonate alteration, respectively. The presence of prehnite-pumpellyite-facies assemblages suggests that these rocks were subjected to an episode of significant retrograde metamorphism. The fact that D_2 affected a pegmatite dyke dated at ca. 2616 Ma within paragneiss units of the Opinaca Subprovince indicates that D_2 was still active at 2616 Ma, and therefore represents a much younger protracted tectono-metamorphic event compared to other events described in the Superior Province, and may share analogies with the extended period of metamorphism from ca. 2682 to 2633 Ma described by Guernina and Sawyer (2003) in the nearly Ashuanipi Subprovince.

Although geochronological work refutes the hypothesis that the Roberto deposit (<2675 ± 6 Ma) is associated with the nearby Ell Lake diorite (2705 ± 1.9 Ma), the potential input from magmatic fluids should not be blindly discarded, as indicated by the presence of potentially younger porphyritic intrusions and multiple generations of pegmatite, some of them being potentially contemporaneous with a part of the mineralization and/or its remobilization.

Compared to most gold deposits of the Abitibi greenstone belt, Roberto is atypical, but like several major gold deposits, it is stratigraphically located above a conglomerate unit in proximity to the contact between two subprovinces. Even though the genetic role played by the kilometre-scale fold is ambiguous, targeting similar fold structures within the region around the Éléonore property, especially near the contact between the Opinaca and La Grande subprovinces, might prove to be a valuable empirical exploration tool. In terms of mineralogical alteration and metamorphic assemblages, calc-silicate-bearing and aluminous assemblages may be proximal to the targeted quartz-microcline-tourmaline-actinolite-diopside-arsenopyrite-pyrrhotite stockworks that host gold mineralization.

ACKNOWLEDGMENTS

This paper is part of a Ph.D. study funded through a Natural Sciences and Engineering Research Council (NSERC) industry grant, the Institut National de la Recherche Scientifique (INRS), the Geological Survey of Canada (GSC), Goldcorp Inc./Opinaca Mines Ltd., and Virginia Mines Inc. The authors would like to thank the entire staff at Opinaca Mines Ltd.'s Éléonore camp for their constant logistical support, and the entire geology team for their significant scientific contribution. Special thanks to N. Prud'homme for her help with managing the large amount of data extracted from the stripped outcrop, to J. Ortega for collaborative fieldwork on the property, and to J. Doyon for sharing her excellent knowledge of the subsurface geology. Thanks to H. Thiboutot (initially at Opinaca Mines Ltd.) for his scientific interest and for his plan to strip the very large outcrop, and to the technical staff that was actively involved in the stripping. Thanks to A. Gaumond and P. Archer at Virginia Mines Inc. for giving the authors the opportunity to undertake the study, and to Virginia Mines Inc.'s geology team for their constructive input. Thanks to D. Bandyayera (Ministère des Ressources naturelles et de la Faune du Québec) and his team for giving the authors the opportunity to be involved in their study and for sharing their knowledge of the regional geology. Thanks to M. Gauthier (Université du Québec à Montréal) for constructive discussions and to P. Mercier-Langevin (GSC) for improving the manuscript. J.-F. Ravenelle would like to thank the Prospectors and Developers Association of Canada (PDAC), the Geological Association of Canada (GAC), and the Consorem for their financial support through scholarships.

REFERENCES

Bandyayera, D. and Fliszár, A., 2007. Géologie de la région de la baie Kasipasikatch (33C09) et du lac Janin (33C16); Ministère des Ressources naturelles et de la Faune du Québec, RP 2007-05, 15 p.

Bécu, V., Ravenelle, J., Malo, M., Dubé, B., Gauthier, M., and Simoneau, J., 2007. Résultats préliminaires de l'étude de la minéralisation Cu-Au-Ag de l'indice du Lac Ell et de ses implications sur la génèse du gisement d'or Roberto, propriété Éléonore, Baie James; Rapport d'étape DIVEX, SC21, 40 p.

Bohlen, S., 1991. On the formation of granulites; Journal of Metamorphic Geology, v. 9, p. 223–229. doi:10.1111/j.1525-1314.1991.tb00518.x

Cadieux, A.-M., 2000. Géologie du gîte aurifère Eau Claire, propriété Clearwater, Baie James, Québec; M.Sc. thesis, Université Laval, Québec, Quebec, 242 p.

Chapdelaine, M. and Huot, F., 1997. Projet Auclair; rapport des travaux, été 1997. Mines d'or Virginia; Ministère des Ressources naturelles du Québec, GM 55428, 113 p.

David, J. and Parent, M., 1997. Géochronologie U-Pb du Projet Moyen-Nord; Ministère des Ressources naturelles du Québec, GM 59903, 88 p.

Doyon, J., 2004. Comparaison de la composition des roches métasédimentaires archéennes dans six bassins de la province du Supérieur: une étude géochimique et statistique; M.Sc. thesis, Université du Québec à Chicoutimi, Chicoutimi, Quebec, 214 p.

Dubé, B. and Gosselin, P., 2007. Greenstone-hosted quartz-carbonate vein deposits; in Mineral deposits of Canada: a synthesis of major deposit-types, district metallogeny, the evolution of geological provinces, and exploration methods, (ed.) W.D. Goodfellow; Geological Association of Canada, Mineral Deposits Division, Special Publication, v. 5, p. 49–73.

Franconi, A., 1978. La bande volcanosédimentaire de la rivière Eastmain inférieure à l'ouest de la longitude 76 (degrés) 15 (min); Ministère des Richesses naturelles du Québec, DPV 574, 177 p.

Franconi, A., 1983. Région de la Gorge Prosper; Ministère de l'Énergie et des Ressources du Québec, MM 82-02, 52 p.

Gauthier, M. and Larocque, M., 1998. Cadre géologique, style et répartition des minéralisations métalliques de la Basse et de la Moyenne Eastmain, Territoire de la Baie James; Ministère des Ressources naturelles du Québec, MB 98-10, 86 p.

Gauthier, M., Larocque, M., and Chartrand, F., 1997. Cadre géologique, style et répartition des minéralisations métalliques de la basse et de la moyenne-Eastmain, Territoire de la Baie James; Ministère des Ressources naturelles du Québec, MB 98-10, 85 p.

Goldcorp Inc., 2010 Goldcorp announces sixth consecutive increase in gold reserves; [press release], http://www.goldcorp.com/news/goldcorp/index.php?&content_id=765 [accessed March 2010]

Goutier, J., Dion, C., Doucet, P., and David, J., 1996. Géologie de la ceinture volcanosédimentaire du Lac Yasinski, sous-province archéenne de La Grande, Baie James; in Séminaire d'information sur la recherche géologique, programme et résumés 1996, Ministère des Ressources naturelles du Québec, DV 96-02, p. 10.

Guernina, S., and Sawyer, E.W., 2003. Large-scale melt-depletion in granulite terranes: an example from the Archean Ashuanipi Subprovince of Quebec; Journal of Metamorphic Geology, v. 21, p. 181–201. doi:10.1046/j.1525-1314.2003.00436.x

Ispolatov, V., Lafrance, B., Dube, B., Creaser, R., and Hamilton, M., 2008. Geologic and structural setting of gold mineralization in the Kirkland Lake-Larder Lake gold belt, Ontario; Economic Geology and the Bulletin of the Society of Economic Geologists, v. 103, p. 1309–1340.

Johnson, T.E., Hudson, N.F.C., and Droop, G.T.R., 2003. Evidence for a genetic granite-migmatite link in the Dalradian of NE Scotland; Journal of the Geological Society, v. 160, p. 447–457. doi:10.1144/0016-764902-069

Jones, K.A. and Brown, M., 1990. High-temperature 'clockwise' P-T paths and melting in the development of regional migmatites: an example from southern Brittany, France; Journal of Metamorphic Geology, v. 8, p. 551–578. doi:10.1111/j.1525-1314.1990.tb00486.x

Kruckenberg, S.C., Whitney, D.L., Teyssier, C., Fanning, C.M., and Dunlap, W.J., 2008. Paleocene-Eocene migmatite crystallization, extension, and exhumation in the hinterland of the northern Cordillera: Okanogan dome, Washington, USA; Geological Society of America Bulletin, v. 120, p. 912–929. doi:10.1130/B26153.1

Labbé, J.-Y. and Grant, M., 1998. Géologie de la région de Lac Natel: (33B/04); Ministere des Ressources naturelles du Québec, RG 98-14, 28 p.

Moukhsil, A., 2000. Géologie de la région des lacs Pivert (33C/01), Anatacau (33C/02), Kauputauchechun (33C/07) et Wapamisk (33C/08); Ministère des Ressources naturelles du Québec, RG 2000-04, 47 p.

Moukhsil, A., Legault, M.I., Boily, M., Doyon, J., Sawyer, E., and Davis, D.W., 2003. Synthèse géologique et métallogénique de la ceinture de roches vertes de la Moyenne et de la Basse-Eastmain (Baie-James); Ministère des Ressources naturelles, de la Faune et des Parcs du Québec, ET 2002-06, 55 p.

Mueller, A. and Groves, D., 1991. The classification of Western Australian greenstone-hosted gold deposits according to wall-rock-alteration mineral assemblages; Ore Geology Reviews, v. 6, p. 291–331. doi:10.1016/0169-1368(91)90008-U

Paquette, L. and Gauthier, M., 1997. Séquences archéennes du Lac Sakami, Baie James; Ministère des Ressources naturelles du Québec, MB 97-02, 40 p.

Percival, J.A., 1989. A regional perspective of the Quetico Meta-Sedimentary Belt, Superior Province, Canada; Canadian Journal of Earth Sciences, v. 26, p. 677–693. doi:10.1139/e89-058

Percival, J.A., 2007. Geology and metallogeny of the Superior Province, Canada; *in* Mineral deposits of Canada: a synthesis of major deposit-types, district metallogeny, the evolution of geological provinces, and exploration methods, (ed.) W.D. Goodfellow; Geological Association of Canada, Mineral Deposits Division, Special Publication, v. 5, p. 903–928.

Poulsen, K., Robert, F., and Dubé, B., 2000. Geological classification of Canadian gold deposits; Geological Survey of Canada, Bulletin 540, 106 p.

Robert, F., 2001. Syenite-associated disseminated gold deposits in the Abitibi greenstone belt, Canada; Mineralium Deposita, v. 36, p. 503–516. doi:10.1007/s001260100186

Robert, F., Poulsen, K.H., Cassidy, K.F., and Hodgson, C.J., 2005. Gold metallogeny of the Superior and Yilgarn cratons; in Economic geology 100th anniversary volume, (ed.) J.W. Hedenquist, J.F.H. Thompson, R.J. Goldfarb, and J.P. Richards; Society of Economic Geologists, p. 1001–1033.

Ryan, R.J. and Smith, P.K., 1998. A review of the mesothermal gold deposits of the Meguma Group, Nova Scotia, Canada; Ore Geology Reviews, v. 13, p. 153–183. doi:10.1016/S0169-1368(97)00017-6

Simard, M. and Gosselin, C., 1999. Géologie de la région du lac Lichteneger: (33B); Ministère des Ressources naturelles du Québec, RG 98-15, 25 p.

Thériault, R. and Bilodeau, C., 2001. Carte géologique du Québec; Ministère des Ressources naturelles du Québec, DV 2002-06, scale 1/2 000 000.

Tremblay, M., 2006. Minéralisation et déformation du gîte aurifère de la zone Eau Claire, propriété Clearwater, Baie James; M.Sc. thesis, Université du Québec à Chicoutimi, Chicoutimi, Quebec, 181 p.

Geological Survey of Canada Project TG6003